Functional Assessment of DFIG and PMSG-based Wind Turbines for Grid Support Applications

Final Project Report

S-73G

Power Systems Engineering Research Center
Empowering Minds to Engineer
the Future Electric Energy System

Functional Assessment of DFIG and PMSG-based Wind Turbines for Grid Support Applications

Final Project Report

Project Team
Zhaoyu Wang, Project Leader
Iowa State University

Graduate Student
Nicholas David
Iowa State University

PSERC Publication 18-08

September 2018

For information about this project, contact:

Zhaoyu Wang
Iowa State University
Electrical and Computer Engineering
1113 Coover Hall
Ames, Iowa 50014
phone: 515-294-6305
email: wzy@iastate.edu

Power Systems Engineering Research Center

The Power Systems Engineering Research Center (PSERC) is a multi-university Center conducting research on challenges facing the electric power industry and educating the next generation of power engineers. More information about PSERC can be found at the Center's website: http://www.pserc.org.

For additional information, contact:

Power Systems Engineering Research Center
Arizona State University
527 Engineering Research Center
Tempe, Arizona 85287-5706
Phone: 480-965-1643
Fax: 480-727-2052

Notice Concerning Copyright Material

Acknowledgements

This project was made possible through support of the Iowa State University Electric Power Research Center (EPRC) and the research initiatives by members of the PSERC. We wish to thank our PSERC industry advisors Patrick Panciatici, Thibault Prevost, and Florent Xavier of RTE-France. We also thank Anne Kimber and Jim McCalley of the EPRC for their support of this work at the ISU Wind Energy Systems Laboratory.

Executive Summary

Wind turbines have massive rotating electrical generators that normally require full or partial coupling to the bulk power system using power electronic converters to control operation and the interconnection. A power system equipped with double-fed induction generators (DFIG) or with permanent magnet generators (PMSG) can have steady-state and transient performance that depends on specific control action and system dynamics. Therefore, the behavior of such controller has a critical role in system stability and dynamic performance of the power system. In addition, the power system is evolving toward a future with many interspersed and interconnected power-electronic based generators and loads. It is important to understand the role and impact of generators as the nature of the system changes. The inherent flexibility of power electronic systems makes them particularly useful in roles of active and reactive power management for grid support.

Although power converters play an important role in the overall performance and reliability of the electric power systems, it is not well understood how controller-influenced dynamics impact the power system. Furthermore, it is important to understand how to make the most use of wind-fueled generators and other power electronic resources to provide ancillary service in voltage and frequency control operations. This project investigates the ability for DFIG and PMSG wind turbines to provide service benefits by studying their theoretical capability and also performing experiments to test dynamics and observe mechanisms of the problem. After studying their capability for ancillary services, we propose a DFIG controller to add service of frequency response. Turbines with PMSGs may also benefit from a similar method. We also propose a DFIG configuration with grid-connected rotor windings to improve reactive power generation capability.

In particular, we find there are three main problems to consider:

1. There is misunderstanding of frequency response capability of DFIG wind turbines. Power electronic coupling is not always similar to full decoupling of frequency and voltage response from generator electromechanical dynamics. We consider the DFIG capability by removing influence of the controller and evaluating inertial response under assumptions of a low-inertia (DFIG-only, self-supporting) power system. We find the machine responds to a load-change in a stable manner and with rotor torque that draws upon stored rotational energy while the mechanical rotor and electrical frequency undergo dynamics. We find that the dynamics of the DFIG-only system give a baseline for developing a physics-based frequency and voltage response control law to provide a level of inherent stability. Linearized response of the DFIG to load transient shows useful ability for frequency response from the rotating turbine.
2. Controllers today are not well-suited for use in low-inertia power systems. In fact, a method of torque and reactive power control alone or even with added droop control might have negative impact on response when considering a low-inertia system. Torque and reactive power (TQ) control and droop-type methods are insufficient for ensuring a stable operation. Response should adapt to the changing load condition in magnitude and time. We propose a control which is derived from a physics-based model to provide inherent stability with response characteristic equations affected by the design choice and with response capability limited by parameters of the turbine and generator.

3. Reactive power capability from power electronic-connected devices is not clear since it depends on converter ratings and also parameters of the interconnecting device. For DFIG wind turbines, reactive power is generated or consumed by the machine-side converter of a back-to-back converter system. Filter inductors and generator windings consume some reactive power and can reduce the overall reactive power generation capability. RTE requires specifically that generators be able to provide reactive power capacity amounting to 1/3 of the nominal real power rating. It is not clear whether some generators can provide this, so this project investigates the capability of the DFIG for reactive power generation. Experiments are performed to illustrate the mechanisms and justify the ability for the converter-based reactive power capability. This project extends the approach and proposes a DFIG connection strategy that can shift the reactive power capability region toward more generation. The ability to provide reactive power consumption and generation even at low and no-wind speeds with full or partial coupling makes power electronic converters useful for reactive power ancillary services.

Power electronic converters have the ability to control the amount of resource being extracted for conversion to electric energy. The behavior of wind turbines with only torque and reactive power control during frequency excursion can be highly improved by advanced controls, especially in situations with low inertia. Frequency responsive controls have often been proposed in some form of a 'droop' or otherwise proportional control which can have the stabilizing effect. The problem is that they do not make a fulfilling use of the resource opportunity and their reliability depends heavily on the scenario. A load-responsive controller is needed to regulate frequency using rotor energy exchange and measured frequency change. This project proposes such controller with frequency and voltage control laws designed using a physics-based model under low-inertia assumptions. It provides a self-stabilizing frequency and voltage response that complements existing torque and reactive power control. The result is a tunable inertial frequency response due to load-change. Capability exists for the frequency and voltage to be maintained for sufficient duration (e.g. 50 % overload for greater than five seconds.) This means that dynamics of load-change can be managed and wind turbines can be used for reliable transient response.

Analytic evaluation of the wind turbine power systems is provided using standard steady-state and dynamic models. Boundaries of the reactive power capability are theorized considering generator parameters and converter and generator nameplate limits. Benefits are estimated for a surveyed set of generators. We find that not all generators exhibit benefit from the proposed rotor-tied configuration, and some show benefit in low-wind compared to high-wind operating conditions. We consider the stability of the DFIG power system using electromechanical dynamics to form transfer functions in the Laplace Domain. Characteristic equations are found to be influenced by power electronic controllers and generator parameters. We then derive a proportional plus integral (PI) control law that stabilizes frequency response due to load change. The proposed controller does not require communication or additional hardware. Rather, it adds a level of transient control not otherwise present. Flexibility of the control parameters spreads capability of the generator for specified depth and duration of response. Poles and zeros of the low-inertia system (i.e. DFIG only) can be specified to provide local stability. Coupled with external and slower primary and secondary controllers, distributed wind turbines can provide a level of frequency response to arrest load transients. A future with response categories and capability requirements can ensure stable long-duration operation.

Beyond theoretical expectation, we find experiments provide further and deeper insight to mechanisms behind the phenomena and lead to advanced understanding of the impact generators have on reliability and resiliency of the power system. A DFIG wind turbine test stand at the wind energy systems lab (WESL) at Iowa State University (ISU) lead to recent discovery of a new DFIG connection scheme that improves efficiency through reduced magnetic core loss. This project extends that work and shows improved value in reactive power generation as well. A PMSG test stand is also being built through this project to better understand the dynamics of PMSG wind turbines and their grid-interactive controllers. The DFIG and PMSG test equipment was useful in providing evidence of inertial response capability, reactive power configuration preference, and frequency control performance.

This work creates future opportunities for adding value to reactive power and frequency response capability. More fulfilled use of wind turbines relieves burden from other generators in the system. These added services from distributed or centralized wind plants could be used to replace auxiliary components like static-var compensators, synchronous condensers, and flywheels. With flexible controls, wind turbines could contribute to frequency and voltage response. They could also help fulfill spinning reserve requirements, or act as a motor load to enhance demand-response. The extendedreactive power generation capability can afford added reactiveconsuming loads. The proposed self-stabilizing frequency control can reduce the frequency response provided elsewhere in the system.

Technical contributions of this project to the art of generator operation include these primary advances:

1. Deeper understanding of DFIG wind turbine frequency response capability of rotor mass, evidenced by a linearization of load-transient response considering a special low-inertia condition.
2. Realization that wind turbines with torque and reactive power control have a locally detrimental impact on frequency response, evidenced by a transient stability analysis considering effect of the DFIG controller in a self-supporting power system.
3. Development and derivation of a self-stabilizing frequency and voltage controller to provide transient response with tunable depth and duration, without added communication or hardware. Control law derivation and stability analysis provide mathematical basis for prescribing response.
4. A DFIG connection strategy that can make improved use of converter and generator nameplate current ratings. The alternative configuration results in a shift of the reactive power capability region; particular designs can benefit from added reactive generation capability. Bounds are equated to illustrate capability based on electrical parameters including resistance and inductance and provide basis for a preferred configuration.
5. Hardware test stands of DFIG and PMSG wind turbines and power electronic converters and controllers, demonstrating phenomena and verifying theory.

Project Publications:

[1] N. David and Z. Wang, "Physical rotor inertia of DFIG wind turbines forshort-term frequency regulation in low-inertia grids," in *2017 IEEE General Meeting*, July 2017.

[2] N. David and Z. Wang, "Rotor-tied configuration of DFIG wind turbines for improving reactive power support capability," accepted for *2018 IEEE General Meeting*, August 2018.

[3] N. David, Z. Wang, F. Xavier, and T. Prevost, "Fast frequency response by DFIG wind turbines for power systems with low physical inertia," in revision, reviewed by *IEEE Transactions on Energy Conversion*.

Student Theses:

[1] Nicholas David. *Availing grid support capabilities of wind turbine generators through configuration and control*, PhD Dissertation, Iowa State University, May 2019 (expected).

Table of Contents

List of Figures

List of Tables

1. Introduction

Wind turbines are often of a type-3 or type-4 configuration having either partial or full power converter interconnection, respectively. The type-3 typically uses a double-fed induction generator (DFIG) with a back-to-back (B2B) power converter rated 1/3 of the total power. The type-4 typically uses a permanent-magnet synchronous generator (PMSG) with a B2B converter rated for full power. Ancillary service capabilities of these systems are not well understood and the impact they have on power system dynamic response can be harmful if care is not taken. Effects of their influence are observed today and there is a timely need for added response capability from wind turbines [1]. As their penetration in the power system continues to rise the need for more reliable operation becomes apparent.

This project is important to the power grid in that it works to improve transient stability of the system. It proposes a controller that makes effective use of the DFIG wind turbine rotor to support short-term power imbalance. A new DFIG configuration is also proposed which can enhance its reactive power generation capability. Voltage and frequency ride-through can be improved and the utility of wind turbines will be increased.

1.1.1 Objectives

This project studies the capability of wind power generators that use power electronic interconnection. This research clarifies discrepancy surrounding claims of steady-state and transient behavior. It provides derivation of theoretical capability using appropriate generator and control models. Transient behavior is also considered for suitability in future power systems having lowered physical inertia. Stability of generator controllers is studied and then improved using a proposed controller. This project provides experimental evidence to support claims made of real and reactive power and transient capability. Specifically, this work has the following objectives:

Derive limits of DFIG reactive power capability. Verify claims of additional capability beyond the current RTE requirement of $\pm 0.3 P_n$ at all conditions. Any limitation observed at low wind speed shall be addressed.

1. Model the characteristics of DFIG and PMSG wind turbines to provide very fast active and reactive power when there is a load change.

Derive a frequency responsive controller to compensate for fast transients that otherwise cause instability. Perform experiments using a controllable lab-scale DFIG and power system to evaluate the transient capability for frequency regulation.

Derive potential for DFIG frequency response to determine if it is possible to rely on inertia provided by DFIG wind turbines to sustain the power system immediately after a fault. Show that it is possible to achieve frequency regulation with wind power.

1.1.2 Benefits to the power system industry

This project will validate control systems to ensure adequate and improved grid-support and control functions. It will increase understanding of limitations and capabilities of wind turbines and increase their functionality and utility in power systems. We will improve the electric service reliability through the use of voltage and frequency control functions offered by wind energy equipment. Another benefit of this work is the contribution to the research laboratory infrastructure. The DFIG and PMSG wind turbine emulators developed in this project can be used in future studies to quantify the impact of advanced controllers on other parts of the power system. The contributions of model validation and controller developments can impact planning and operational aspects of the broader power system. The work enables future studies of multi-machine networked microgrids, distributed generation and energy management, demand response, flexible-ac systems, and more. Specific outcomes of this project include:

- Experiments proving mechanisms of electromechanical wind power systems.
- Derivations and test procedures for estimating wind turbine generator capabilities.
- Modeling equations and stability analysis for use in wind powered systems.
- Example of DFIG response maintaining frequency during load perturbations.
- Validated claims of DFIG reactive power support capability.
- Derived DFIG frequency response without control influence, proving existence of capability.
- Simulation of islanding condition that proves instability of common DFIG controllers.
- Derived frequency controller to contribute an inherent and tunable fast frequency response.
- Lab test equipment for continued work on integration of renewable energy power systems.

1.2 Background

Wind turbines with DFIGs and power electronic (PE) converters are common generators. Turbines with PE converters have the ability to control real and reactive power at the generator terminals independently. Wind turbine generators and their capabilities are not completely understood. There is room to make better use of the renewable energy resources to improve power system performance. This project aims to improve our understanding of turbine-grid interactions and operating limitation. There are three main aspects to consider:

i. Reactive power capability and its contribution to voltage response.

   A discrepancy exists between claimed and measured DFIG reactive power capability and requires investigation. We provide a derivation considering generator parameters and provide case studies to illustrate mechanisms and identify limitations. We propose an improvement of the generation capability using an alternative terminal connection strategy (grid-connected rotor instead of grid-connected stator).

ii. Real power capability and its link to rotor kinetic energy and electrical frequency.

There are misconceptions regarding DFIG capability for frequency response in high-wind power systems. We investigate the response mechanisms of electromagnetic coupling between the grid and the generator rotor mass. Tests are performed on a generator that has a hub-emulating flywheel to illustrate the phenomena of load-transient frequency response.

iii. Suitability of wind turbine controllers for beneficial grid support.

Controllers that operate today may not be suitable for aiding the transition to future power systems that have many wind turbines and PEs. We study the effect of grid-following torque and reactive power controllers and prove that they contribute a harmful effect to frequency response. The art of wind turbine control can be advanced with added frequency response capability. Response time can be improved and ride-through capability enhanced. Control methods that rely on communication for coordinating the turbine's response lack resiliency. We propose a generator control architecture that provides a fast frequency response component and allows a specified balance of electrical and mechanical dynamics (deviation of grid frequency and rotor speed) without added communication.

DFIG reactive power capability is a function of the generator design and use. Nameplate ratings give some limit of operation, but the connection of the DFIG in the wind turbine system also plays a role. The generator can operate with either the rotor or stator connected to the grid. They key is that the machine must be magnetized in order to transfer torque. Which terminal is grid-connected vs which is converter-connected is found in this project to make a considerable difference. In the conventional configuration where the stator is grid-connected, the frequency in the stator is maintained at the specified grid frequency and the rotor frequency is controlled by the converter to generate specific torque and reactive power. If the grid is applied to the rotor terminals, then the rotor has a constant grid frequency and the frequency of current in the stator varies with converter control. When using the power converter to push or pull reactive power through the generator, a nameplate current limit is eventually reached. The question is which limit, stator or rotor, is the limiting factor in how much reactive power can be transferred. These boundaries are derived in this project and it is shown that the new configuration with a grid-connected rotor can lead to enhanced reactive power generation capability for some machines.

It is important for wind turbine generators to be locally stable to observed load-change. We show here that in low-inertia power system they are unstable using conventional controls. It is not acceptable for them to rely on external resources to afford stable transient response. We provide method to stabilize response to load-change using well-suited controls designed from physics-based models. Self-stabilizing control creates ability for distributed stabilizing response with tuned depth and duration and with limitation of its capability. Adding a service of stabilizing frequency response can reduce the need for inertial and primary response from other generators.

Frequency response defined in [2] is useful. Response characteristics of "inertial", "immediate", "bidirectional", "continuous", and "sustained" are considered valuable and essential. The DFIG controller proposed here exhibits these with prescribed response. Illustrated in Figure 1.1 are four periods in which to consider frequency response, each with appropriate resources and response methods [3]. This paper proposes response in a period acting before primary methods, indicated by the region in the dotted line.

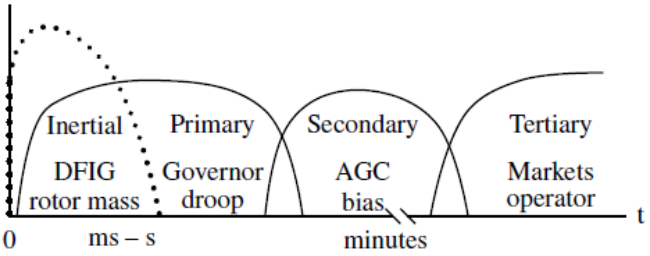

Figure 1.1 Power system frequency control periods. Proposed response by DFIG rotor mass (dotted line) is continuous and extends into the primary range.

In the U.S.A., North American Electric Reliability Corporation (NERC) publishes frequency response performance standards to guide design and operation of generation equipment. Regional transmission operators (RTOs) and Balancing Authorities (BAs) may have performance limits alternate to these at specific generators and substations to meet broader goals.

NERC Standard BAL-001-2 aims to keep transmission interconnection frequency within defined limits [4]. It provides performance calculation of area control error (ACE). NERC Standard BAL-003-1.1 requires BAs to provide ability to arrest and support frequency deviations [5]. BAs are members of Reliability Organizations, such as Midwest Reliability Organization, and may have member utilities or be utilities or RTOs themselves. Generation, transmission, and load may be used to satisfy frequency response obligation (FRO) [6]. NERC Standard PRC-024-2 ensures generator protection relays operate within defined frequency and voltage limits [7]. These relays may have time delays of 12 cycles or more [8]. NERC Standard PRC-006-2 provides limits for over and under-frequency load shedding [9]. Under-frequency is 58 Hz for 2 s, sloping to 59.3 Hz after 60 s. Over-frequency is 61.8 Hz for 2 s, sloping to 60.7 Hz after 30 s. NERC Standard PRC-010-2 allows varied limits for load shedding programs, and coordinates their design and operation [10]. For DFIG wind turbines to provide sufficient response, they shall maintain operation within bounds using only their own capability.

In this paper, response is evaluated on merits of frequency nadir and its time of occurrence, and arrested frequency. Area control error (ACE) combined with measured frequency change, Δf, is a measure of generator contribution to frequency response. A similar performance measure between scheduled and actual power and frequency used here is

$$ACE\Delta f = \left(P_{s,\mathrm{sch}} - P_{s,\mathrm{act}}\right)\left(f_{e,\mathrm{act}} - f_{e,\mathrm{sch}}\right). \tag{1.1}$$

Providing ACEΔf < 0 kW·Hz contributes to regulation. The DFIG control proposed in this project exhibits this behavior.

1.2.1 Related work

In DFIG wind turbines, conventionally the grid is applied to the stator and the machine-side converter (MSC) to the rotor. The MSC normally controls generator torque and grid-side terminal (GST) reactive power, and the grid-side converter (GSC) controls the dc-link voltage and generator converter terminal (GCT) reactive power [11]. The proposed inverse configuration has a grid-connected rotor and the MSC applied to the stator, using identical GSC and MSC; it is referred to

as the rotor-tied configuration (RTC). Alternative machine designs specific to this new configuration were made with objective to result in wound rotor induction machines (WRIM) of lesser volume, using the core material more effectively [12] – [13]. It was also proposed for application to wind turbine energy conversion systems with improved efficiency due to reduced hysteresis loss in the generator core [14] – [15]. An alternative definition of slip was proposed in [16], unique only to this new configuration. Reactive power capability in the RTC has not been studied but is suspected to provide enhanced generation capability. This project explores that capability.

In the field of power electronic DFIG wind turbine control, specifically for provision of frequency response, the current state-of- art has yet to achieve a means of fast frequency response by a controller that works to respond to load change and provide frequency regulation using stored energy in the rotor mass. Activity in this field has increased recently as generators with large physical inertia are replaced by wind turbines and other low-inertia PE-interfaced sources. Yet, a gap exists in our knowledge of DFIG wind turbine frequency response capability, and opportunities exist to enhance their frequency response capability via novel control techniques. A range of DFIG wind turbine steady-state, primary, and secondary controls are available and range in complexity and performance, e.g. [11] – [15]. A selection of these and other DFIG wind turbine controllers proposed for frequency response are summarized for their general qualities and performance capability in Table 1.1. Grid-forming controllers have constant frequency commands and the output is used to either drive the converter frequency ($\omega_e - \omega_r$) or switching angle ($\theta_e - \theta_r$) directly. Those types can suffer from current harmonics that may affect turbine efficiency. Cascaded designs that use frequency deviation to operate on either power P^* or torque T_e^* are inherently slower than their inner power or torque controllers, thus they cannot provide fast inertial response. Fast phase-locked-loops (PLLs) can be used to enhance the ability of cascaded control, but are not always practical [17]. Several layers of control are used in [18] with the components adding to one torque command, using droop, rate of change of frequency (ROCOF), rotor speed, and a sub-optimal maximum power point (MPPT) steady-state component. The existing art demonstrates that rotor speed can be linked to grid frequency deviation by appropriate control, even when the turbine and power system are fully separated by PEs [11], [19], [20].

Some controllers operate on torque or power commands with slow cascaded control and may have operating power headroom requirements [13], [18], [21] – [22]. A direct voltage and frequency control adjusting voltage commands is in [23], although current harmonic distortion can increase. A controller using trajectory generation to replace vector control is proposed in [24] but requires coordination with other sources via communication.

Although attempts have been made to provide a self-stabilizing frequency response controller for DFIGs, there are flaws with the existing methods. Furthermore, many controllers proposed in literature have not had experimental validation. A comparison of the state of art in frequency-responsive control is provided in Table 1.1. Controllers made for grid-forming operation may not be widely applicable. Those that require communication may not work when communication is lost during an outage. Cascaded frequency controllers that operate on power or torque commands may have relatively slow response time and can exhibit deep frequency nadir. Operating directly on converter voltage, frequency, or angle can induce harmonics in the generator current. Primary response for under-frequency events requires sub-MPPT pre-transient operation, limiting energy

generation, and it is ineffective in the 'inertial' time range. A fast-acting controller that links rotor inertia to frequency deviation is sought to complement existing generator controls.

Table 1.1 Attributes of state-of-art inertial frequency response controllers

Controller	General features	Fast & Inertial	Signal acting on	Grid-forming/ following
[16]	Virtual rotor angle from proportionally controlled frequency with constant f^*.	Y	θ_e - θ_r	Form
[25]	Direct stator voltage control, virtual converter angle with constant f^*, no PLL.	Y	v_c^*	Form
[21]	Alters converter frequency, standalone with constant reference f^*, current i^* from rotor speed control.	Y	ω_e - ω_r	Form
[18]	Applies droop, ROCOF, sub-opt. MPPT, and speed control to one torque command.	N	T_e^*	Follow
[13]	GE's WindINERTIA; cascaded and uses droop gain based on available power, includes washout filter.	N	P^*	Follow
[11]	Wind turbines linked to HVDC to grid with VSC, frequency response linked to J via B2B converter, adds integral control of frequency.	N	P^*	Follow
[17]	Uses 2 PLLs – one fast for inertial response, multiplies i_{MPPT}^* with an I-f droop.	Y	i^*	Follow
[19]	Offshore wind with DC-link and VSC, links f_e to J via B2B, GSC alters v_{dc} and MSC translates Δv_{dc} to added ΔP^*.	N	v_{dc}^*, P^*	Follow
[20]	Offshore wind with HVDC and VSC, links f_e to J via B2B, I-f droop acts directly on converter voltage v^* added through a LPF with constant f_e^*.	Y	v_c^*	Form
NEW	Follows low-frequency grid dynamics, PI controller adds to i_{MPPT}^*, control easily design seperately from and to be faster than TQ control, washout filter limits impact, ues simple PLL.	Y	i*	Follow

This project is unique in that we consider generator electromechanical dynamics with special consideration for low-inertia system characteristics. Aerodynamic blade performance is not considered but may influence overall turbine response. We focus on studying the capability of the rotor mass to support load change and associated DFIG control techniques and influence on

frequency response. We reveal the cause and mechanics of transient frequency instability by deriving appropriate linearized transfer functions and provides experimental validation to support its claims.

This project goes beyond simulations and theoretical calculations with work based on experiments and practice. It fills gaps in existing knowledge and art and spurs intrigue with alternative methods. The unique contributions of this project are i) to use hardware setups to test and validate existing models and control methods of various wind turbines in providing grid ancillary services, the results could prove/disprove existing methods and assumptions, and ii) to propose better active/reactive power control techniques for wind turbines to provide voltage and frequency regulation.

1.3 Overview of problems

This project addresses a unique need for wind power to provide power system support functions. Generation resources are not well understood nor are they fully utilized. Improved use and ability of these systems can support evolution toward wind-powered and power electronic-based systems. This project provides solutions based on functional assessments that visualize phenomena. It articulates a rigorous derivation of capability and designs physics-based solutions. Contributions to inertial frequency response and reactive power capability are made.

There are two main components to this problem. The first concerns confusion around reactive power capabilities of wind energy systems, especially during low-wind speed conditions. A second concerns the interaction of turbine and power system during power imbalance. Whether real and reactive power capability of wind turbines can be relied on to provide voltage and frequency support during a synchronous network disturbance is not understood. More specifically, the primary problems include:

- A discrepancy exists between claimed and measured DFIG reactive power capability.
- Misconceptions exist regarding capability of DFIG rotor inertia to provide frequency response in power system with high wind penetration.
- A gap exists in DFIG control capability applicable to low-inertia power systems.
- PMSG wind turbine control is an emerging technology with potential for enhancement.

1.3.1 Frequency Response Issues

The difficulty of power systems with high penetration of power electronic (PE) generation is that sufficient physical inertia must exist to maintain frequency during the sensing, detecting, activating, and start of primary response by auxiliary generators and/or control systems; on the scale of tens to hundreds of milliseconds. With PE-interfaced generation, angular stability may be compromised by its response time and control actions.

The most critical challenge is that PEs require time to measure signals and process data, beginning response after a few hundred milliseconds. Energy storage systems (ESS) and photovoltaics (PV) are expected in high numbers for primary and secondary response but are not continuous nor

immediate. A study in [26] suggests droop-type inertia emulation can be effective for up to 95 % wind turbine penetration; the last 5% is synchronous generation for inertia. Existing controllers are insufficient for 100 % DFIG wind power. The effect is observed in the ERCOT power system, where wind is required to provide 5% frequency-droop if able to. That system response has improved 'B-value' value (arrested stable frequency) but even lower 'C-value' (nadir); the reason is unexplained [1]. Analysis shown in this paper suggests a common DFIG control scheme may contribute to instability.

DFIG and PMSG-based wind power systems may be capable of providing active power and speed control capabilities to support frequency regulation in synchronous networks. How fast and for what duration these frequency control capabilities can be implemented is not well understood. Furthermore, PMSGs for wind turbines are typically designed for low rotor speeds. With these considerations it is desirable to evaluate the potential of frequency support functions on an experimental basis.

We suspect that popular wind turbine controls in use today are unsuitable for supporting a fully wind-powered power system. Controllers of torque and reactive power are not intended to provide stable load-transient frequency response. Traditionally, frequency response is provided by heavy synchronous machines that inherently provide enough response to compensate for detrimental effects of some wind turbines. Although some proposed controllers provide reasonable support today, including droop-type methods, it is only because of the frequency support of other generators in the system that they are afforded stable operation. This project shows that such controllers are actually unstable when the DFIG is solely responsible for the frequency response of a local load. The problem is made evident here when considering islanding operation. Many studies in the literature simply simulate a limited number of specific case-studies and draw conclusions without a solid mathematical basis. Stability analysis is derived in this project and shows the mechanisms of instability under certain control laws.

To fix the problem of unstable frequency response, we develop a generator control architecture that enables well-suited frequency control based on physics of system. Derivation and experiments show the stabilizing response. The proposed control offers self-stabilizing responce for inherent load-transient support. A high-level sketch of the added controller is shown in Figure 1.2. No change is made to the existing torque and reactive power controllers or current controllers. Voltage and frequency commands originate from filtered grid measurement made with a conventional phase-locked loop (PLL) and converter voltage is generated using space vector modulation.

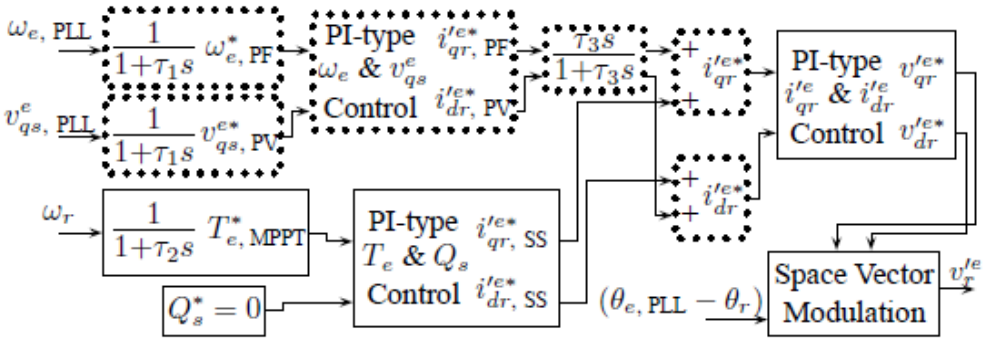

Figure 1.2 High-level diagram of proposed FV controller to complement existing TQ scheme.

The additional frequency and voltage (FV) components complement the existing TQ controllers and add a level of fast-acting response to transients and with low-frequency effect washed out to allow return to pre-transient torque and reactive condition upon restoration by primary response. It has benefits of being continues and immediate, temporary and tunable, and with no added hardware or communication.

1.3.2 DFIG Reactive Power Issues

A primary challenge of renewable energy based power systems is the provision of voltage and frequency ancillary services [27] [28]. Wind turbines with squirrel-cage induction generators offer no control and actually consume reactive power. To support high penetration of function-lacking resources, it is desirable to have additional reactive power "generation" from DFIG wind turbines, but without adding power factor correction (PFC) capacitors which can inadvertently introduce unstable nodes. We propose a generator configuration that offers a solution to improve reactive power range without need for added hardware or communication. It adds value to existing infrastructure and enables higher penetration integration of reactive-consuming and unity-power factor (UPF) renewable energy resources. With added reactive power support we can improve low-voltage transient response [29].

Discrepancies exist between manufacturers and investigators regarding reactive power capabilities of DFIGs, especially at low wind speeds. This has led to the need for independent evaluation of proposed reactive power control schemes and limitations in wind power systems. RTE currently requires a reactive power range of $\pm 0.3 P_n$ (nominal, rated power) regardless of the active power. This work will investigate the reactive power capabilities of wind turbine power converters at low active power. The possibility to extend the allowable reactive power range could allow additional reactive current injection to increase voltage reliability, for example during voltage dip. We will perform tests to evaluate the capabilities of wind turbine generators. Power electronic converters will be used to control reactive power while following typical power vs speed curves of wind turbines. We identify the range of attainable reactive power for the test machines, following nameplate ratings. Experiments will identify any difficulties encountered in implementing reactive power control systems.

Case studies are made to consider capability of specific generators. Experiments are performed on a 7.5 kW laboratory DFIG to validate the proposed derivation and theoretical limitations. Formulas

describing reactive power limitations are applied to a range of machines and benefit from the RTC is observed.

We have particular interest in the RePower MM82 2.0 MW wind turbine. It uses a common DFIG, the VEM brand model DASAA 5025-4UA [30]. This generator accounts for approximately 30 % of the RTE wind capacity and its reactive power capability has come into question. The manufacturer has undergone a redesign to improve capability, but limitation still exists at low wind speed. In this project we study the reactive power capability considering generator electrical parameters and generator and converter nameplate voltage and current ratings. We find in this work that the generator should be capable of producing the required reactive power even at low wind speed. This result concurs with results of another third-party study initiated by RTE [31]. Possible mechanisms creating the discrepancy are identified in our study. They include possibly an insufficient converter voltage or excessively large MSC filter inductance.

1.3.3 PMSG Capability Issues

Wind turbines with permanent-magnet synchronous generators (PMSG) are connected to the power system through a full-power converter. The capability for frequency response is thought to exist. The controlled link of electrical and mechanical load-transient response has similar characteristics to that of the PE-connected DFIG. PMSG wind turbines are typically low-speed machines and so there is question whether they have enough available stored energy to sustain power systems during power imbalance and provide reactive power at low-wind.

A similar control architecture as proposed for the DFIG may enhance the PMSG turbine capability by providing a fast-acting transient-responsive control component that complements the existing steady-state torque and reactive power controllers. In this project, we focused efforts on the process of modeling wind turbine generators and their associated controllers. The controller designed for the DFIG wind turbine is based on an architecture we believe can be applied to many types of PE converters, not just the DFIG or PMSG wind turbine. Papers submitted to journals that cover this field have gained interest of reviewers and revisions to those texts and the added contributions sought have extended the planned amount of time spent on those project aspects. Contributions developed through consideration of DFIG-based wind turbines are expected to apply to PMSG turbines in a similar way. Functional assessment of PMSG wind turbines beyond this PSERC project is continued through the EPRC.

1.4 Report organization

DFIG reactive power capability is considered in section 2. Details of a physics-based model suited to application in DFIG-powered systems is provided. Limits of reactive power generation and consumption are derived based on generator electrical parameters and nameplate voltage and current rating. An alternative connection strategy is proposed to increase the amount of reactive power generation available. Section 3 considers frequency response capability. A model of the DFIG wind turbine is used to consider low-inertia power systems with dynamic electrical frequency. Stability of the system during load-change is derived to include consideration of control mechanisms; destabilizing response is observed. A transient-responsive controller is proposed

there to augment existing steady-state controllers. A design process that uses transfer function methods is provided to specify the frequency and voltage response. Section 4 concludes this work.

2. DFIG Frequency Response Capability

Effects of low-inertia power systems are not widely understood. Dynamic models and control designs need special attention for application in low-inertia power systems. This section discusses fundamentals of low-inertia power systems as applied to DFIG wind turbines.

In this section we first analyze the capability of DFIG wind turbines to provide frequency response. We then propose a PI-type frequency and voltage (FV) control addition to complement existing torque and reactive power (TQ) controllers. Unlike existing frequency response methods, it follows low-frequency grid dynamics and contains a washout filter to limit inertial response and allow return to normal operation. It draws on elements of the existing art but applied in a novel way. It follows low-frequency grid dynamics and provides fast proportional plus integral response to frequency error, giving ability to tune both intensity and duration of response with capability of sustained support limited by physical inertia. A washed-out current component adds to existing current commands already corresponding to MPPT operation, so frequency response can be made faster than torque control without impacting long-term interference between the two. The resulting temporary torque deviation supports load change.

Specific objectives of this section are to 1) provide analytic and experimental evidence about frequency stability of DFIG wind turbines in low-inertia power systems, 2) derive torque control influence on transient frequency stability in response to load step, 3) propose a frequency-responsive DFIG controller to complement existing controllers, 4) perform experiments of utility-connected and islanding-mode inertial frequency response using a micro-scale DFIG wind turbine emulator (rated power of 10 HP) equipped with a hub-emulating rotor flywheel 5) improve the value and utility of Type-III wind turbines.

2.1.1 Modeling stability of DFIG wind turbines in low-inertia power systems

A realistic power system to evaluate DFIG wind turbine inertial support capability is illustrated in Figure 2.1.

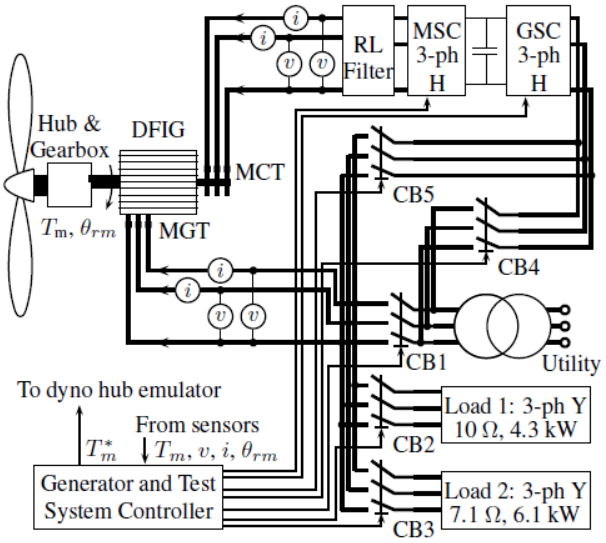

Figure 2.1 High-level schematic of the DFIG and power system.

The DFIG is utility-connected by circuit breaker CB1. Local loads are connected to the stator through CB2 and CB3. CB4 and CB5 allow GSC influence to be either neglected or considered in the response capability. Resistive loads are connected at the stator-side of circuit breaker CB1 via CB2 and CB3 to test the ability of supporting over-load conditions via inertial energy reserves and specific control strategies. The DFIG is controlled by a machine-side converter (MSC) with dc-link controlled by a grid-side converter (GSC). In the analytic consideration of electromechanical inertial frequency response provided herein, influence of the GSC is not considered. Focus is drawn on coupling between the stator windings and rotor mass. Generator control relies on voltage and current sensing at the machine-grid terminal (MGT) and current sensing at the machine-converter terminal (MCT), thus always measuring frequency at the local load. Current is defined positive into the machine. Opening circuit breaker CB1 causes the load to be 100 % dependent on DFIG frequency response. It is assumed that utility generation is composed of additional sources providing inertial, primary, and secondary response, such as synchronous generators, PE-connected PV, ESS, and other wind turbines and inertial sources. Interaction with the utility power system is considered experimentally in effort to prove beneficial capability even when applied in a multi-machine higher-inertia power system. The hub and gearbox assembly provide rotor mass which is emulated by a rotor flywheel driven by a dynamometer.

Commonly cited p.u. inertia, H, has units of s (seconds), whereas physical inertia, J, has units of kg·m^2. The two are related by $J = S_b H P^2/(2\omega_b{}^2)$, where S_b is the per-unit generator power base (S_{rated}) and ω_b is the power system angular frequency base, $\omega_b = 2\pi 60$ rad/s. Thermal synchronous generators have $H \approx 6$–12 s, whereas DFIG wind turbines have $H \approx 2$–3 s. PV and ESS have $H = 0$ s. In systems with characteristically low inertia, ω_e may accelerate rapidly; it cannot be considered constant. Physical inertia, J, impacts rotor acceleration according to

$$\frac{2}{P} J \frac{d\omega_r}{dt} = T_e + T_m - D\omega_r, \tag{2.1}$$

where D is mechanical damping. In the control period, the rotor and hub assembly is assumed stiff. Power system dynamics and MSC operation influence electromagnetic torque, T_e. Mechanical torque applied by the wind, T_m, is constant and corresponds to electrical rotor speed ω_r for MPPT

$$T_m = \frac{1}{2}\rho C_p A \left(\frac{r}{g\lambda}\right)^3 \left(\frac{2}{P}\omega_r\right)^2. \tag{2.2}$$

Herein, consider a DFIG wind turbine with swept area A of radius $r = 2.25$ m, gear ratio $g = 4.4$, and a constant tip-speed ratio $\lambda = 8$. It operates with a wind speed range $v_w = [4, 12]$ m/s which corresponds to the slip range $S = [0.5, -0.5]$. Stator and rotor terminal power are related to mechanical shaft power and slip by:

$$P_s = \frac{-P_m}{1-S} \tag{2.3}$$

$$P_r = -SP_s, \tag{2.4}$$

where slip is defined as

$$S = \frac{\omega_e - \omega_r}{\omega_e}. \tag{2.5}$$

Generation is implied when $T_e < 0$, $P_s < 0$, and $P_r < 0$. In low-inertia grids, this partial PE coupling means DFIG and MSC dynamics both play a critical role in governing ω_r.

DFIG control is normally performed in the synchronous reference frame (SRF), having *q*-axis aligned with stator voltage and *d*-axis 90° behind [32]. The MSC establishes the rotor voltage vector using space vector modulation (SVM) while the PLL measures $v_{qs}^e = V_{\text{grid}}\sqrt{2/3}$, $v_{ds}{}^e = 0$ V, and $\theta_e = \int \omega_e \, dt$. MSC *qd* voltage and current commands are dc in steady-state and correspond to angle $(\theta_e - \theta_r)$. A shaft encoder measures $\omega_{rm} = (2/P)\omega_r$. MSC frequency has value $(\omega_e - \omega_r)$ which is an artifact of the PLL following the stator voltage angle. In low-inertia grids, *qd* control accelerates the synchronous reference frame, i.e. the stator voltage vector. Physics-based electrical dynamic equations of the DFIG are derived in [32]. They are summarized in (2.6) – (2.9) with (2.10) made to consider a loose stator frequency. This means the DFIG is driving the system. The model is useful to consider single-turbine capability, but may not be applicable to multi-machine systems with other sources for electrical frequency change.

$$v_{qs}^e = r_s i_{qs}^e + \omega_e \lambda_{ds}^e + p\lambda_{qs}^e \tag{2.6}$$

$$v_{ds}^e = r_s i_{ds}^e - \omega_e \lambda_{qs}^e + p\lambda_{ds}^e \tag{2.7}$$

$$v_{qr}'^e = r_r' i_{qr}'^e + (\omega_e - \omega_r)\lambda_{dr}'^e + p\lambda_{qr}'^e \tag{2.8}$$

$$v_{dr}'^e = r_r' i_{dr}'^e - (\omega_e - \omega_r)\lambda_{qr}'^e + p\lambda_{dr}'^e \tag{2.9}$$

$$p\omega_e = p\omega_r \tag{2.10}$$

where *p* is derivative operator and stator and rotor flux are

$$\lambda_{qs}^e = L_{ls} i_{qs}^e + L_M\left(i_{qs}^e + i_{qr}'^e\right) \tag{2.11}$$

$$\lambda_{ds}^e = L_{ls} i_{ds}^e + L_M(i_{ds}^e + i_{dr}'^e) \tag{2.12}$$

$$\lambda_{qr}'^e = L_{lr}' i_{qr}'^e + L_M\left(i_{qs}^e + i_{qr}'^e\right) \tag{2.13}$$

$$\lambda_{dr}'^e = L_{lr}' i_{dr}'^e + L_M(i_{ds}^e + i_{dr}'^e). \tag{2.14}$$

Now instead of ω_e being assumed constant, ω_r, and $(\omega_e - \omega_r)$ are free to vary and accelerate in response to control action. In the synchronous reference frame stator real and reactive power are

$$P_s = \left(\frac{3}{2}\right)\left(v_{qs}^e i_{qs}^e + v_{ds}^e i_{ds}^e\right) \tag{2.15}$$

$$Q_s = \left(\frac{3}{2}\right)\left(v_{qs}^e i_{ds}^e - v_{ds}^e i_{qs}^e\right). \tag{2.16}$$

and electromagnetic torque is

$$T_e = \left(\frac{3}{2}\right)\left(\frac{P}{2}\right)\left(\lambda_{ds}^e i_{qs}^e - \lambda_{qs}^e i_{ds}^e\right). \tag{2.17}$$

Dynamics of (2.7) – (2.10) allow design of linear time invariant (LTI) proportional plus integral (PI) current controllers which make the MSC stator-referred voltage commands

$$v'^{e*}_{qr} = \left(i'^{e*}_{qr} - i'^{e}_{qr}\right)K_{\mathrm{i}}\left(1+\frac{1}{\tau_{\mathrm{i}}s}\right) + \frac{L_M}{L_s}v^{e}_{qs} - \frac{L_M}{L_s}r_s i^{e}_{qs} - \omega_r L_M i^{e}_{ds} + (\omega_e - \omega_r)L'_r i'^{e}_{dr} - \omega_e \frac{L_M^2}{L_s} i'^{e}_{dr} \tag{2.18}$$

$$v'^{e*}_{dr} = \left(i'^{e*}_{dr} - i'^{e}_{dr}\right)K_{\mathrm{i}}\left(1+\frac{1}{\tau_{\mathrm{i}}s}\right) + \frac{L_M}{L_s}v^{e}_{ds} - \frac{L_M}{L_s}r_s i^{e}_{ds} + \frac{L_M}{L_s}\omega_e \lambda^{e}_{qs} - (\omega_e - \omega_r)\sigma L'_r i'^{e}_{qr} - (\omega_e - \omega_r)\frac{L_M}{L_s}\lambda^{e}_{qs}, \tag{2.19}$$

where $\sigma = 1 - L_M^2/(L_s L_r')$. Current control ensures sinusoidal current in the generator. Commands normally originate from TQ controllers also designed in the Laplace domain,

$$i'^{e*}_{qr,\mathrm{T}} = \frac{\lambda^{e}_{qs} i'^{e*}_{dr}}{\lambda^{e}_{ds}} + (T_e - T_e^*)K_{\mathrm{T}}\left(1+\frac{1}{\tau_{\mathrm{T}}s}\right) \tag{2.20}$$

$$i'^{e*}_{dr,\mathrm{Q}} = \frac{\lambda^{e}_{ds}}{L_M} + (Q_s - Q_s^*)K_{\mathrm{Q}}\left(1+\frac{1}{\tau_{\mathrm{Q}}s}\right). \tag{2.21}$$

Parameters $K_{\mathrm{T,Q}}$ and $\tau_{\mathrm{T,Q}}$ achieve specified poles and zeros of the current control transfer function. The problem of angular instability is first illustrated by the MSC space-vector diagram in Figure 2.2. Rotor current normally resides in the quadrant shown with $T_e > 0$ Nm and $Q_s = 0$ var; super-synchronous speeds have $v_{qr}{}'^{e} < 0$. Generating torque is produced by $i_{qr}{}'^{e} > 0$, and $i_{dr}{}'^{e} > 0$ provides MSC reactive power generation.

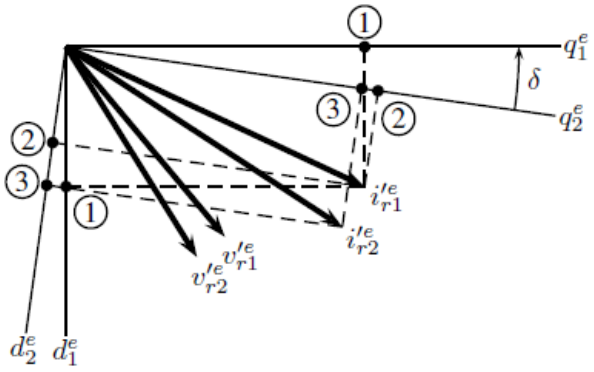

Figure 2.2 Power system load increase represented by a voltage angle step at the DFIG stator terminals. Here $\delta = -8^{\circ}$ and vectors are enlarged for affect.

Consider a load increase approximated by a voltage angle step, $\delta < 0$, at the generator stator terminals. MSC voltage angle steps from $v_{r1}{}'^{e}$ to $v_{r2}{}'^{e}$. Current and torque measurements immediately step with the apparent angle change measured by the PLL. MSC current moves from $i_{r1}{}'^{e}$ to $i_{r2}{}'^{e}$ according to machine and control dynamics. Apparent load-induced angle-step causes the immediate increase of measured $i_{qr}{}'^{e}$ and thus measured value of T_e. The current controller responds relatively fast, and torque control more slowly. The torque controller responds to apparent need for a step-changed torque reduction by reducing the current command. This actually causes reduction of T_e in response to the initial load increase. Consider the initial *qd* currents at point 1 in Figure 2.2 when a load increase creates a voltage phase shift at the stator terminals. Current then appears to have value at point 2 and quantities in (2.1) and (2.6) – (2.17) change accordingly. When the reference frame shifts from $q_{d1}{}^{e}$ to $q_{d2}{}^{e}$, (2.18) and (2.19) quickly act to follow the phase shift. TQ control apparently also needs to accelerate currents from point 2 to 3 by

(2.20) and (2.21), but do so more slowly and without consideration of stator response. In low-inertia grids, this further acceleration is too rapid for reliable operation. The next subsection provides a derivation to prove capability for stable response when TQ controls are removed.

2.1.2 Proof of capability for stable frequency response due to load change

A mechanism of instability is action of the generator TQ controller. Yet, the capability for stable frequency response during load-transient exists. It is evident when the influence of the TQ and current controllers is neglected. In the generator controller, a phase-locked-loop (PLL) measures the grid voltage magnitude and frequency. The integration of the PLL frequency provides the transformation angle between *abc* and *qd* reference frames. The PLL response is considered much faster than all controllers and its effect on transient response is negligible. Current control may also produce unstable effect, but it too is relatively fast. Furthermore, it is undesirable to change the current controller as it ensures sinusoidal current. We can prove the capability for stable load response by ignoring influence of the TQ and current controllers and linearizing the DFIG model. Rotor speed and stator frequency deviation at T_{dur} are estimated by the linearization of T_e in (2.1). DFIG dynamics are derived in [32]. Voltage equations in terms of rotor and stator flux, machine parameters, and equivalent stator load, R_L, are

$$v_{qs}^{e} = \frac{\omega_e \lambda_{ds}^{e}}{1+a} + p\frac{\lambda_{qs}^{e}}{1+a} \tag{2.22}$$

$$v_{ds}^{e} = \frac{-\omega_e \lambda_{qs}^{e}}{1+a} + p\frac{\lambda_{ds}^{e}}{1+a} \tag{2.23}$$

$$v_{qr}^{\prime e} = \frac{r_r^{\prime}\lambda_{qs}^{e}}{L_M} + \frac{r_r^{\prime}L_s}{r_s L_M}\left(\frac{a}{1+a}\right)\omega_e \lambda_{ds}^{e} + (\omega_e - \omega_r)\lambda_{dr}^{\prime e} + p\left(\frac{r_r^{\prime}L_s}{r_s L_M}\right)\left(\frac{a}{1+a}\right)\lambda_{qs}^{e} + p\lambda_{qr}^{\prime e} \tag{2.24}$$

$$v_{dr}^{\prime e} = \frac{r_r^{\prime}\lambda_{ds}^{e}}{L_M} - \frac{r_r^{\prime}L_s}{r_s L_M}\left(\frac{a}{1+a}\right)\omega_e \lambda_{qs}^{e} - (\omega_e - \omega_r)\lambda_{qr}^{\prime e} + p\left(\frac{r_r^{\prime}L_s}{r_s L_M}\right)\left(\frac{a}{1+a}\right)\lambda_{ds}^{e} + p\lambda_{dr}^{\prime e}, \tag{2.25}$$

where p is the derivative operator, d/dt , $a = r_s/R_L$, and

$$\lambda_{qs}^{e} = \mathrm{L_s i_{qs}^{e}} + \mathrm{L_M i_{qr}^{\prime e}} \tag{2.26}$$

$$\lambda_{ds}^{e} = \mathrm{L_s i_{ds}^{e}} + \mathrm{L_M i_{dr}^{\prime e}} \tag{2.27}$$

$$\lambda_{qr}^{\prime e} = \mathrm{L_r^{\prime} i_{qr}^{\prime e}} + \mathrm{L_M i_{qs}^{e}} \tag{2.28}$$

$$\lambda_{dr}^{\prime e} = \mathrm{L_r^{\prime} i_{dr}^{\prime e}} + \mathrm{L_M i_{ds}^{e}}. \tag{2.29}$$

Electromagnetic torque in terms of flux only is

$$T_e = \left(\frac{3P}{4}\right)\left(\frac{L_M}{L_s L_r^{\prime} - L_M^2}\right)\left(\lambda_{qs}^{e}\lambda_{dr}^{\prime e} - \lambda_{ds}^{e}\lambda_{qr}^{\prime e}\right). \tag{2.30}$$

Stator load change creates a change of flux, thereby changing torque, rotor speed, and stator frequency. Pre-transient conditions are denoted by subscript 0, and post-transient by subscript T. R_L at time t_0 and t_T are

$$R_{L0} = \left(\frac{3}{2}\right)\frac{v_{qs0}^{e2}}{P_{s0}} \tag{2.31}$$

$$R_{L\mathrm{T}} = \left(\frac{3}{2}\right)\frac{v_{qs0}^{e2}}{P_{s\mathrm{T}}}. \tag{2.32}$$

The equivalent change in load parameter *a* is

$$\Delta a = \frac{r_s}{R_{L\mathrm{T}}} - \frac{r_s}{R_{L0}}. \tag{2.33}$$

Arranging (2.22) – (2.25) for flux in terms of *qd* stator voltage and frequency, rotor speed, machine parameters, and equivalent stator load allows linearization of electromagnetic torque about the operating point. Change of torque is computed by finding the change of flux due to stator load change; $\Delta\lambda(a) = \lambda'(a_0)\Delta a$, where $\lambda'(a_0)$ is the partial derivative of λ with respect to *a* and evaluated at the initial condition.

For example, (2.22) is arranged as

$$\lambda_{ds}^{e} = \frac{v_{qs}^{e}}{\omega_e} + \frac{v_{qs}^{e} a}{\omega_e}. \tag{2.34}$$

The change of λ_{ds}^{e} due to change of *a* is

$$\Delta\lambda_{ds}^{e} = \frac{v_{qs0}^{e}}{\omega_{e0}}\Delta a. \tag{2.35}$$

Similar operations are performed for (2.23) – (2.25), leading to

$$\Delta\lambda_{qs}^{e} = \left(\frac{-v_{ds0}^{e}}{\omega_{e0}}\right)\Delta a \tag{2.36}$$

$$\Delta\lambda_{dr}^{\prime e} = \left(\frac{r_r' L_s \lambda_{ds0}^{e}}{r_s L_M s_0}\right)\left(\frac{a_0}{(1+a_0)^2} - \frac{1}{1+a_0}\right)\Delta a \tag{2.37}$$

$$\Delta\lambda_{qr}^{\prime e} = \left(\frac{r_r' L_s \lambda_{qs0}^{e}}{r_s L_M s_0}\right)\left(\frac{a_0}{(1+a_0)^2} - \frac{1}{1+a_0}\right)\Delta a. \tag{2.38}$$

Change of electromagnetic torque is computed with respect to the change of all flux components

$$\Delta T_e = \left(\frac{3P}{4}\right)\left(\frac{L_M}{L_s L_r' - L_M^2}\right)\left(\lambda_{dr0}^{\prime e}\Delta\lambda_{qs}^{e} + \lambda_{qs0}^{e}\Delta\lambda_{dr}^{\prime e} - \lambda_{qr0}^{\prime e}\Delta\lambda_{ds}^{e} - \lambda_{ds0}^{e}\Delta\lambda_{qr}^{\prime e}\right). \tag{2.39}$$

From (2.1), rotor speed deviation over the period $\mathrm{T_{dur}}$ is

$$\Delta\omega_r = \Delta T_e \frac{P}{2J}\mathrm{T_{dur}} \tag{2.40}$$

and the stator electrical frequency deviation by

$$\Delta\omega_e = \frac{-\Delta\omega_r}{(s_0 - 1)}. \tag{2.41}$$

At $t = T_{dur}$, the electrical rotor speed and stator frequency are

$$\omega_{rT_{dur}} = \omega_{r0} + \Delta\omega_r \tag{2.42}$$

$$\omega_{eT_{dur}} = \omega_{e0} + \Delta\omega_e. \tag{2.43}$$

Frequency deviation for load steps of ± 1, 5, and 10 % of nominal MPPT at each wind speed are calculated. Results for T_{dur} = 200 ms are plotted in Figure 2.3. The stator frequency remains well within its bounds.

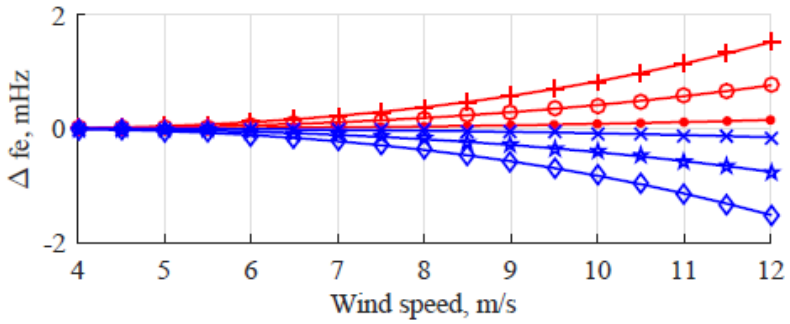

Figure 2.3 Linearized stator frequency deviation 200 ms after a ±1 % (x/·), 5 % (⋆/◦), and 10 % (⋄/+) load change for a turbine with inertia J = 2.65 kg·m^2.

Consider the time-domain response when the TQ and current controllers are disabled. During a test, when a 10 % load increase is made at the stator terminal, the converter *qd* output voltage commands and PLL measured stator frequency are simultaneously latched to the pre-transient value. This makes the converter voltage angle remain fixed with respect to the load. When a load is added the result is an increased angle separation between the converter and grid voltage vectors, inducing power flow and rotor torque. Simulated response for a 10 % load increase at rated speed and power is pictured in Figure 2.4. Stator load is switched at t = 0.01 s. Generator torque increases and the rotor slows down.

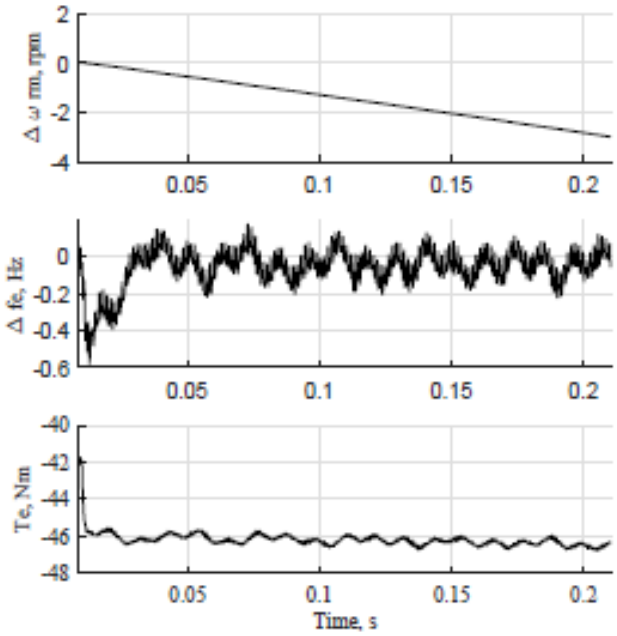

Figure 2.4 Simulated rotor speed, stator PLL-measured frequency, and electromagnetic torque due to a 10 % load increase from rated speed and power.

Effects of a load change are observed by the PLL as a frequency impulse. Without action of any controllers, voltage angle separation naturally increases generator torque to match the load demand. This is analogous to the torque increase of a synchronous generator due to angle separation of the stator voltage and internal electromotive force.

2.1.3 Proof of unstable frequency response from TQ control

We can prove that action of the TQ controllers initiate an unstable frequency response and that slowing their response can be helpful but insufficient alone. For this purpose, the transfer function of frequency change with respect to change of electromagnetic torque is derived. Parameters of the TQ controllers are included in the response.

Proof of the mechanisms behind instability is revealed by the linearized transfer function of frequency response due to apparent change of torque command, H(s) = $\Delta\omega_e$(s)/ΔT_e^*(s). To link effects of physical inertia and controller influences, (2.21) is used with (2.17), (2.10) and (2.5). The resulting swing equation is

$$\frac{2J}{P}\frac{d\omega_e}{dt} = \frac{3P}{4}\left(\lambda_{ds}^e i_{qs}^e - \lambda_{qs}^e i_{ds}^e\right) + T_m - D(1-S)\omega_e \tag{2.44}$$

Rotor and stator currents are related using (2.11) and (2.12). Current control response is fast enough to be neglected, so one can assume $i_{qr}{}'^e = i_{qr}{}'^{e*}$ and $i_{dr}{}'^e = i_{dr}{}'^{e*}$, yielding

$$\frac{2J}{P}\frac{d\omega_e}{dt} = \frac{3P}{4}\left(\frac{\lambda_{ds}^e\lambda_{qs}^e}{L_s} - \frac{\lambda_{ds}^e L_M}{L_s} i_{qr}^{e*} - \frac{\lambda_{qs}^e\lambda_{ds}^e}{L_s} + \frac{\lambda_{qs}^e L_M}{L_s} i_{dr}^{e*}\right) + T_m - D(1-S)\omega_e. \tag{2.45}$$

Including TQ controller influence of (2.20) and (2.21), then

$$\frac{2J}{P}\frac{d\omega_e}{dt} = \frac{3P}{4}\left(-\frac{\lambda_{ds}^e L_M}{L_s}\left(\frac{\lambda_{qs}^e i_{dr}'^e}{\lambda_{ds}^e} + (T_e - T_e^*)K_{\mathrm{T}}\left(1+\frac{1}{\tau_{\mathrm{T}}s}\right)\right) + \frac{\lambda_{qs}^e L_M}{L_s}\left(\frac{\lambda_{ds}^e}{L_M} + (Q_s - Q_s^*)K_{\mathrm{Q}}\left(1+\frac{1}{\tau_{\mathrm{Q}}s}\right)\right)\right)$$

$$+T_m - D(1-S)\omega_e. \tag{2.46}$$

From (2.6), $\lambda_{ds}^e \approx v_{qs}^e/\omega_e$ and (2.7) $v_{ds}^e \approx 0$, reactive power response is neglected and (2.46) reduces to

$$\frac{2J}{P}\frac{d\omega_e}{dt} = -\frac{3Pv_{qs}^e L_M}{4L_s}\omega_e^{-1}T_e\left(K_{\mathrm{T}} + \frac{K_{\mathrm{T}}}{\tau_{\mathrm{T}}s}\right)$$

$$+\frac{3Pv_{qs}^e L_M}{4L_s}\omega_e^{-1}T_e^*\left(K_{\mathrm{T}} + \frac{K_{\mathrm{T}}}{\tau_{\mathrm{T}}s}\right) + T_m - D(1-S)\omega_e. \tag{2.47}$$

Transient stability is evaluated by considering small changes made by the electromechanical system and by control action. Linearizing (2.47) about the operating point, the partial derivatives $d\mathrm{f}(\omega_e, T_e^*) = (\partial \mathrm{f}/\partial\omega_e)d\omega_e + (\partial \mathrm{f}/\partial T_e^*)dT_e^*$, considering that in steady-state $(T_e - T_e^*) = 0$, are

$$\frac{\partial f}{\partial \omega_e} = -D(1-S) \tag{2.48}$$

$$\frac{\partial f}{\partial T_e^*} = \frac{3Pv_{qs}^e L_M}{4L_s\omega_e}\left(K_{\mathrm{T}} + \frac{K_{\mathrm{T}}}{\tau_{\mathrm{T}}s}\right). \tag{2.49}$$

Therefore, the linearized swing equation in the Laplace domain is

$$\frac{2J}{P}\mathrm{s}\Delta\omega_e = -D(1-S)\Delta\omega_e + \frac{3Pv_{qs}^e L_M}{4L_s\omega_e}\left(K_{\mathrm{T}} + \frac{K_{\mathrm{T}}}{\tau_{\mathrm{T}}\mathrm{s}}\right)\Delta T_e^* \tag{2.50}$$

and the transfer function is

$$\frac{\Delta\omega_e}{\Delta T_e^*} = \frac{3P^2 v_{qs}^e L_M K_T}{8JL_s\omega_e}\frac{\left(s+\frac{1}{\tau_{\mathrm{T}}}\right)}{\mathrm{s}\left(\mathrm{s}+\frac{D(1-S)P}{2J}\right)} \tag{2.51}$$

with v_{qs}^e, ω_e, and S evaluated at the initial operation condition. The system has one zero at $s_{z,\mathrm{T}} = -1/\tau_{\mathrm{T}}$, one pole at $s_{p1,\mathrm{T}} = 0$ rad/s and a second pole at $s_{p2,\mathrm{T}} = -D(1-S)/(2J)$. The system is unstable due to the pole at the origin. Both physical inertia, J, and torque control parameters K_{T} and τ_{T} contribute to the magnitude and rate of response. Damping D is usually small (e.g. the laboratory DFIG system has $D = 2.74\times10^{-4}$ kg·m^{2}rad^{-1}s^{-1}) making the second pole also close to the origin. Torque control time constant τ_{T} moves the zero, to a limited extent; a torque response slower than the AGC command is undesired. Slowing the torque controller can improve response, but cannot practically be made slow enough without also impacting pitch and primary response systems. Not studied in detail but considered possible is to also speed up the blade pitch response so the incoming wind is governed for rotor speed regulation. In that way the torque controller could be slowed enough to allow the presence of inertial response, as speculated in the simulation of section 2.1.2.

Time-domain frequency response for stepped load change is evaluated by simulating an islanding condition with a local stator-connected resistive load, in a configuration similar to that of Figure 2.1 but with different load. To evaluate the inertial coupling of rotor mass to stator load, GSC response is neglected by simulating its ac-connection to an arbitrary energy source (e.g. CB5 open and CB4 closed). Cases of TQ-only designs and also a droop method of frequency response are studied. For clarity, responses considered herein use a current controller illustrated in Figure 2.6 with input filter time constant τ_1 = 0.227 ms and poles overdamped and centered at -400 rad/s. Space vector modulation switching frequency is 7 kHz, and T_e^* originates by low-pass filtered (LPF) measurement of rotor speed with filter time constant τ_5 = 0.1 s.

Table 2.1 TQ control designs and their frequency response

set	τ_2 (ms)	$s_{pT,Q}$ (rad/s)	$s_{zT,Q}$ (rad/s)	$f_{e,\,\mathrm{nadir}}$ (Hz)	t_{nadir} (ms)	$f_{e,\,\mathrm{t=0.2\ s}}$ (Hz)
A	22.7	-60, -20	-30, -40	54.53	24.9	215.6
B	22.7	-6, -2	-3, -4	53.81	30.9	87.67
C	22.7	-0.6,-0.2	-0.3, -0.4	53.72	31.9	76.87
D	22.7	-5.1, -2	-0.6, -20	52.01	40.5	58.65
E	227	-1, -2	-0.5, -4	36.31	377.4	41.22
F	22.7	Case E + 5 % droop		54.2	20.9	57.7

Control designs of

Table 2.1 are simulated for an islanding response with a 10 % load increase. The response is shown in Figure 2.1 and shows that stator frequency is indeed unstable due to effect of weakening T_e, meaning the rotor does not contribute well to frequency response. Cases A–D have $\Delta\omega_{rm} > 0$ rpm, which means they actually respond with load rejection instead of load support. The increased load demand at the stator terminals upon utility disconnection is observed by the controller PLL as a voltage angle step as described in Figure 2.2, and appearing in measurement of T_e as a brief torque increase. Frequency initially appears to drop, but the apparent sudden torque increase initiates torque controller response at the same time. As torque response continues, instability occurs. Instead of responding with frequency support, the rotor speed remains nearly unchanged and action of the torque controller accelerates the electrical frequency.

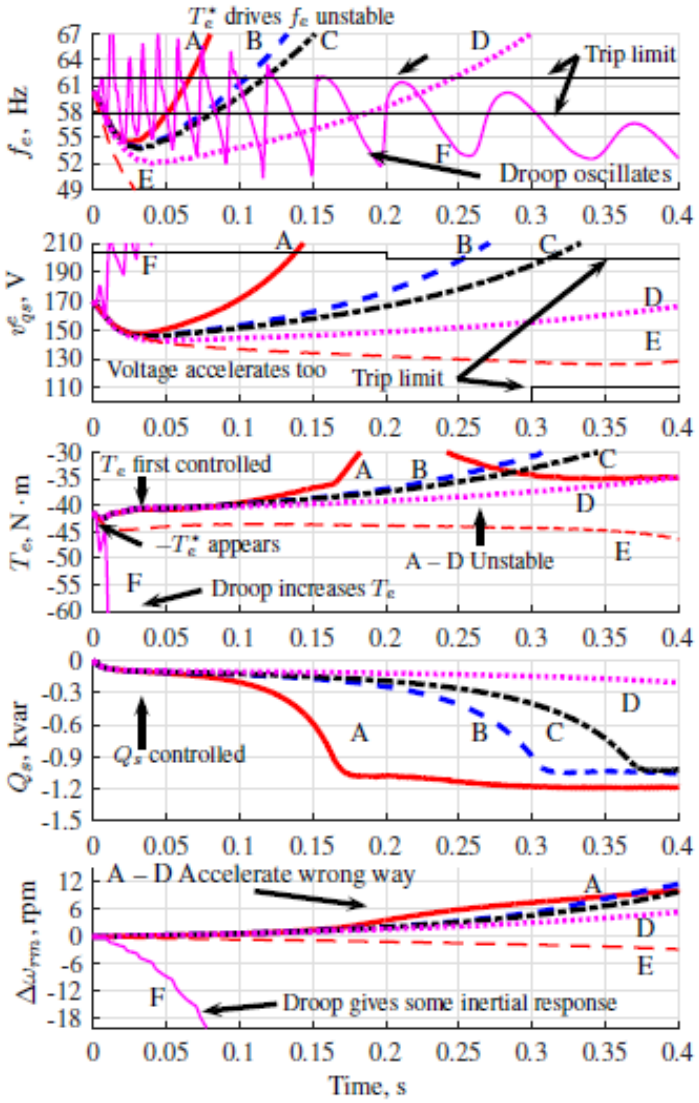

Figure 2.5 Inertial response to a 10% load increase with 100 % reliance on DFIG inertial frequency response. Plotted are TQ-only control designs made fast (A, solid), slow (B, dashed), slower (C, dot-dashed), slow with high damping (D, dotted), slow with lower filter (E, thin dashed), and with 5 % droop (F, oscillating solid).

Control speed (pole placement) of the TQ controllers affects the duration and intensity of frequency response. Fast control, case A, results in fast acceleration of f_e. Slowing response to cases B and C improves duration but lowers nadir. Additional damping in case D also has impact. Case E has slower control input filters which slows and stabilizes response but with unacceptable frequency deviation; some inertial response is observed in ω_{rm}. Case F applies a 5 % frequency droop control. Again some inertial contribution is observed in ω_{rm} but so too are unacceptable oscillations in f_e. Using the popular TQ control, physical inertia is under-utilized, and frequency response is reliable for less than 20 ms.

Turbines using only TQ control effectively have negative contribution to inertial frequency response. Although today there exists enough inertia and sufficiently active primary response from other generators to compensate; that may not always be the case, nor does it have to be.

Because the TQ controllers naturally induce an unstable frequency response, they are actually placing undue burden on other power system stabilizing equipment. It would be preferred to have wind turbine generators that are capable of stabilizing their own response. In this way, they could effectively contribute to regulation of frequency and voltage during load-change. A set of frequency and voltage responsive controllers is proposed in the next section to counter the harmful affect.

2.2 Proposed generator control to stabilize transient response

A key point of the proposed solution is that it provides a means of temporarily counteracting the degrading effects of TQ control with an additional component of current command to provide prescribed grid-following frequency regulation. The proposed control addition easily integrates with the existing TQ controller and provides near zero steady-state frequency error into the primary control period. The FV controllers ensure regulation to pre-fault values. The control addition links load transients to the generator rotor speed and converter voltage. A schematic of the control addition is drawn with dashed lines in Figure 2.6. No changes to the existing TQ controller is necessary, although slowing their response is shown to have positive impact.

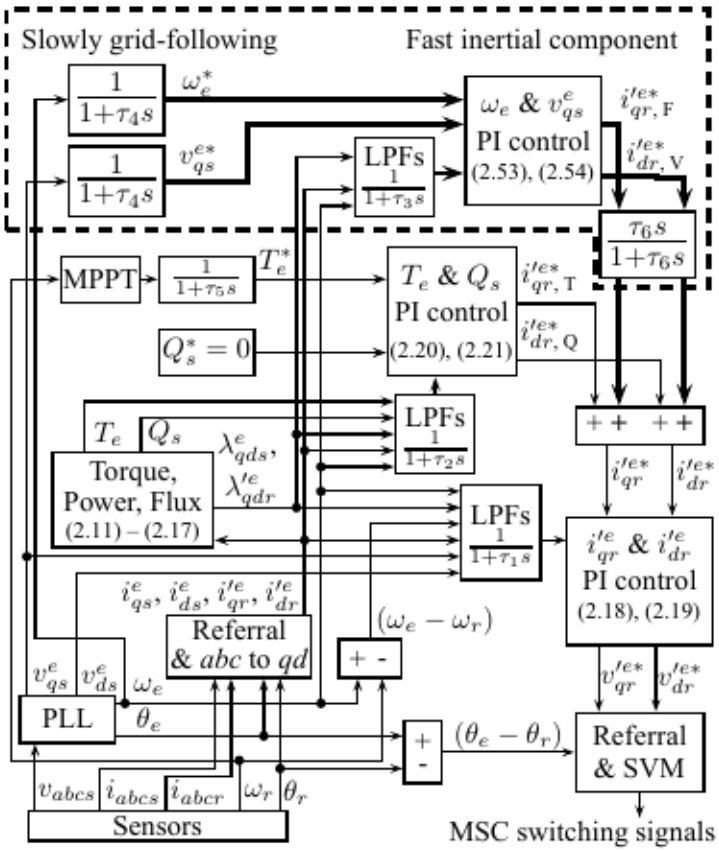

Figure 2.6 Proposed inertial frequency control addition (dashed outline).

Our proposed control is a second set of PI-controlled current commands added to those of the TQ commands to support new load. For example, Figure 2.7 shows how the torque controller's current command accelerates the wrong direction, and how the proposed "inertial" component of current command counteracts that effect to change torque and satisfy new load.

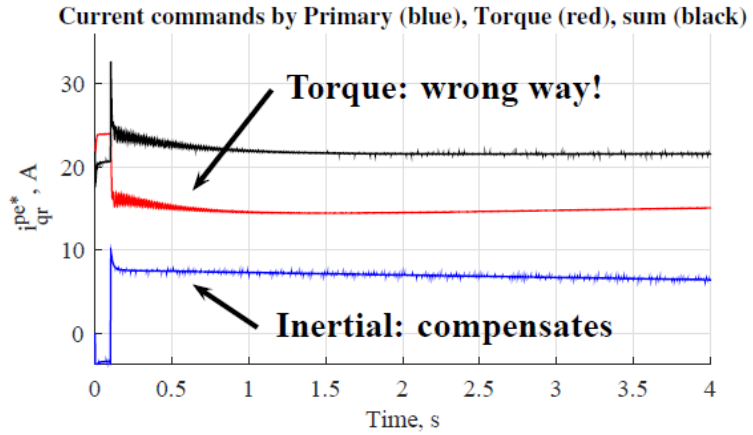

Figure 2.7 The proposed control addition (blue) counteracts the unstable effect of torque control.

Gains are based only on generator parameters and tuned for desired response. A high pass filter (HPF) limits bandwidth of response, allowing only temporary excursion from normal TQ operation in response to load change. The proposed controller acts to regulate frequency via energy exchange with the rotor mass. It provides a tunable balance of transient appearance in mechanical and electrical dynamics. Commands f_{e^*} and v_{qse^*} are obtained from LPF stator measurement. A filter time constant of $\tau_4 = 15$ s aligns with a typical period within which automatic generation commands (AGC) for primary frequency response are provided by balancing authorities. In this way, slower deviation and primary response from other units are still followed.

We derive the proposed control law using only the DFIG dynamic equations. The frequency controller has a current command $i_{qr,\mathrm{F}}{}^{'e*}$ derived from (2.6), neglecting current/flux dynamics (assuming the current controller provides accurate and fast control) and using (2.11) and (2.7) to arrange for rotor current as a linear time invariant (LTI) function of frequency. Similarly, voltage control has a current command $i_{dr,\mathrm{V}}{}^{'e*}$ derived from (2.6) and using (2.12) written for a function of voltage. The generator q-axis rotor current as a function of angular frequency is

$$i'^{e}_{qr} = \left(\frac{r_s i^e_{ds} - v^e_{ds}}{L_M \omega_e}\right) - \frac{r_s v^e_{qs}}{r_s L_M} + \frac{L_s \omega_e \lambda^e_{ds}}{r_s L_M}. \tag{2.52}$$

The current commands of the frequency and voltage responsive components are thus defined with feed-forward terms based on the generator model and PI control to compensate for the system dynamics, as

$$i'^{e*}_{qr,\mathrm{F}} = (\omega^*_e - \omega_e) K_{\mathrm{F}} \left(1 + \frac{1}{\tau_{\mathrm{F}} s}\right) + \frac{r_s i^e_{ds}}{\omega_e L_M} - \frac{v^e_{ds}}{\omega_e L_M} - \frac{v^e_{qs} L_s}{r_e L_M} \tag{2.53}$$

$$i'^{e*}_{dr,\mathrm{V}} = \left(v^{e*}_{qs} - v^e_{qs}\right) K_V \left(1 + \frac{1}{\tau_{\mathrm{V}} s}\right) - \frac{r_s i^e_{qs}}{\omega_e L_M} - \frac{i^e_{ds} L_s}{L_M}. \tag{2.54}$$

The resulting controller transfer functions are

$$\frac{\omega_e(\mathrm{s})}{\omega_e^*(\mathrm{s})} = \frac{K_\mathrm{F}(\tau_\mathrm{F}\mathrm{s}+1)}{\left(\frac{L_s\lambda_{ds}^e}{r_s L_M}+K_\mathrm{F}\right)\tau_\mathrm{F}\mathrm{s}+K_\mathrm{F}} \tag{2.55}$$

$$\frac{v_{qs}^e(\mathrm{s})}{v_{qs}^{e*}(\mathrm{s})} = \frac{K_\mathrm{V}(\tau_\mathrm{V}\mathrm{s}+1)}{\left(\frac{1}{\omega_e L_M}+K_\mathrm{V}\right)\tau_\mathrm{V}\mathrm{s}+K_\mathrm{V}} \tag{2.56}$$

Gains $K_{\mathrm{F,V}} > 0$ and $\tau_{\mathrm{F,V}} > 0$ s are defined to place the pole and zero of each, as

$$K_\mathrm{F} = \frac{\frac{s_\mathrm{pF}}{s_\mathrm{zF}}L_s\lambda_{ds}^e}{\left(1-\frac{s_\mathrm{pF}}{s_\mathrm{zF}}\right)r_s L_M} \tag{2.57}$$

$$K_\mathrm{V} = \frac{\frac{-s_\mathrm{pV}}{s_\mathrm{zV}}}{\left(\frac{s_\mathrm{pV}}{s_\mathrm{zV}}-1\right)\omega_e L_M} \tag{2.58}$$

$$\tau_\mathrm{F,V} = \frac{-1}{s_\mathrm{zF,V}} \tag{2.59}$$

The response of the FV controllers should be designed to complement the TQ controllers. This means the FV controllers should have their response designed to be sufficiently faster than the TQ controllers. The effect of the FV control should be to counter the destabilizing effect of TQ controllers. Because the transient FV control decays with time via the washout filter, there is limited interference with the more steady-state TQ control.

The addition of the separately derived and designed FV and TQ current command components provides the ability for the FV response to be made faster or slower than the TQ response. The intensity and bandwidth can be asserted by relative pole/zero placement and control filter τ_3. The duration of response is influenced by input-command filter τ_4 and washout filter τ_6.
Instead of specifying the amount of generator effort in response to observed transient and accepting the resulting frequency response, we can now specify what the response should look like so the generator is designed to adapt responding effort.

2.2.1 Stable response from combined effects of TQ and FV control

Since both T and F control operate on the same current command, it is possible for them to interfere. However, we can design their respective individual transfer functions to mitigate interference. In fact frequency response can be made fast enough to provide reliable frequency stability and with low-frequency response washed out to limit response. The derivation of frequency response due to load step and including control influence with the added washed-out inertial components is similar to derivation of (2.51), and is useful to prove the stabilizing properties of the proposed control addition.

The transfer function of frequency response including all control influence can be derived. Starting from the swing equation of (2.45), we substitute the current commands $i_{qr}{}'^{e*}$ and $i_{dr}{}'^{e*}$ with the sum of those output variables from the TQ and FV controllers. The resulting transfer function is

$$\frac{\Delta\omega_e}{\Delta T_e^*} = \frac{\frac{\alpha K_{\mathrm{T}}}{\omega_e}\left(\mathrm{s}+\frac{1}{\tau_{\mathrm{T}}}\right)\left(\mathrm{s}+\frac{1}{\tau_6}\right)}{\frac{2J}{P}s^3+\left(\frac{2J}{P\tau_6}+\gamma+\frac{\alpha v_{qs}^e L_s}{\omega_e^2 r_s L_M}\right)\mathrm{s}^2+\left(\frac{\gamma}{\tau_6}-\frac{\alpha K_{\mathrm{F}}}{\omega_e}\right)\mathrm{s}-\frac{\alpha K_{\mathrm{F}}}{\omega_e \tau_{\mathrm{F}}}}, \tag{2.60}$$

where $v_{qs}{}^e$, ω_e, $\gamma = 3Pv_{qs}{}^eL_M/(4L_s)$, and $\alpha = D(1 - S)$ are evaluated at the initial operating condition. The system has two zeros and three poles. Interestingly, the zeros are placed by the torque controller and high-pass filter (HPF) designs, and the poles placed by the frequency controller design. Although the HPF introduces another pole and zero, it provides ability to specify frequency response to be faster than torque response. We can strategicly place the relative poles and zeros to limit influence of the inertial component and allow return to $T_e{}^*$ e and $Q_s{}^*$ upon subsidence of inertial response and return to scheduled frequency. The response is tuned via the mix of PI gains for stable, damped, and satisfying inertial frequency response. The stability of the voltage response can also be derived and may be interesting when considering reactive power transients. Here, the stability of the voltage response is ensured by design of the transient voltage controller and reactive power change is not considered. We experimentally analyze the benefits of power system integration using the proposed controller in the next section.

2.3 Testing the proposed DFIG transient response

Experiments of utility-connected and islanding operation are performed under several proposed control designs and load-transient conditions. The low-inertia DFIG test system is photographed in Figure 2.8 and with components and connections as in Figure 2.1. It consists of an 1800 rpm 7.5 kW DFIG with an 86 kg steel flywheel attached to the rotor shaft, achieving $H \approx 2.2$ s. Generator electrical parameters may be found in [33]. This machine has rotor and stator terminals with similar voltage rating. Hence, the DFIG and local zero-inertia resistive loads are coupled to the utility via a two-winding isolating transformer. The generator is driven by a dynamometer using a torque-control mode with constant torque T_m for the duration of study. Two dSPACE ds1103 controllers run the system.

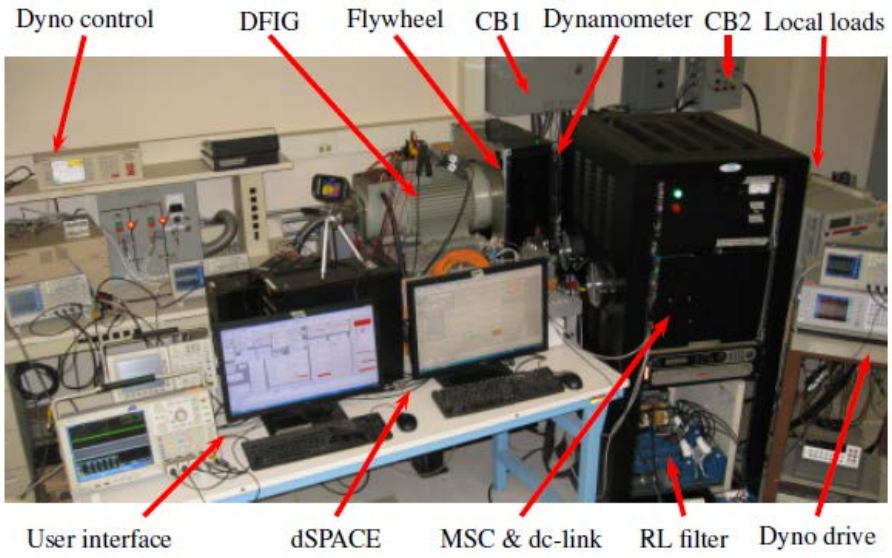

Figure 2.8 Low-inertia power system test stand with a 7.5 kW DFIG and hub-emulating flywheel, dynamometer, PE converters, and zero-inertia resistive loads.

We perform tests to provide evidence of inertial frequency response capability. Change in T_e and ω_{rm} is evidence of the inertial response to load change; rotor kinetic energy is drawn upon to support the electrical load. Tests are performed to evaluate response for a) utility-connected load-change support without influence of the GSC, b) islanding local load support without GSC influence, and c) islanding support with the GSC connected to the stator terminals.

2.3.1 Utility-connected load-transient support with proposed control

When CB1 is closed, local load is well supported by the high-inertia utility connection provided at the laboratory. Support from the DFIG for local load change is still provided to the observed transient. Pictured in Figure 2.9 is the utility-connected response to local 6.1 kW resistive load increase while ω_{rm} = 1630 rpm ($P_{s,\,\mathrm{MPPT}}$ = 4.3 kW), for several control sets in Table 2.2.

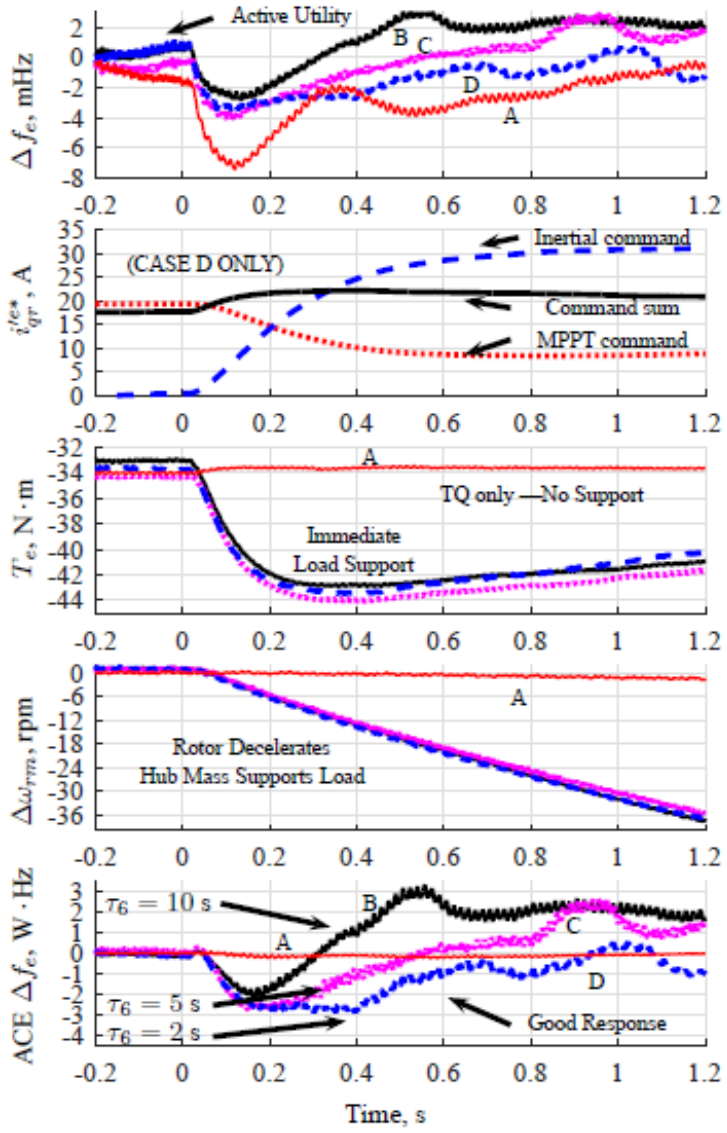

Figure 2.9 Utility-connected inertial response to local 6.1 kW load increase, for control cases in Table 3.1. *Note:* Periodic utility loads exist and also initiate some transients.

Case A is TQ-only control, and B–I are FV control with various pole, zero, and washout settings according to Table 3.1 in the next subsection. Compared to TQ-only control case A, the proposed controller provides superior inertial frequency response that is immediate and according to design. FV current commands counteract those created by TQ controllers so the resulting command temporarily supports load change. Rotor speed and steady-state TQ operation are restored upon decay of inertial response and return to scheduled frequency. Cases of Figure 2.9 are shown for an extended duration in Figure 2.10.

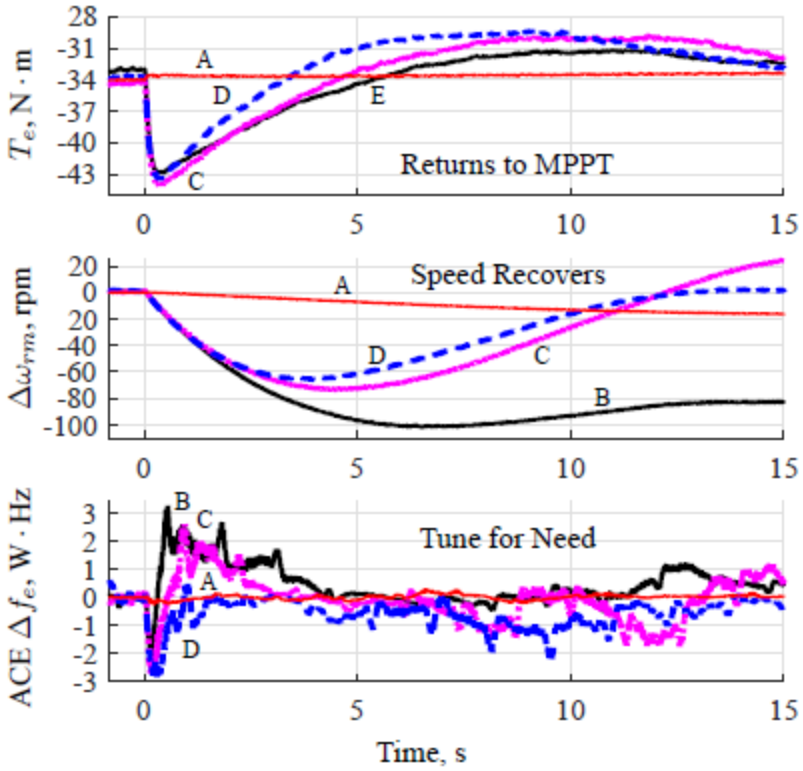

Figure 2.10 Long-term utility-connected inertial response to local 6.1 kW load increase. Response is temporary and balanced according to design.

Temporary load support is provided while allowing return to MPPT operation. Evidenced by ω_{rm} and ACEΔf_e, response contribution by rotor mass varies according to design, particularly with washout filter τ_6. Smaller τ_6 (case D) allows higher-frequency control effort and thus faster grid-following. Larger τ_6 (case B) extends the duration of response; too small and it interferes with AGC and primary response. All are improvements from case A. The decreased rotor speed may affect the aerodynamics of the wind turbine. Impact on mechanical torque may prolong speed recovery.

2.3.2 Islanding support of proposed inertial response via MSC, without GSC

The inertial frequency response via stator electromagnetic rotor coupling is evaluated with local load-change by performing a low-inertia islanding test. The system is modeled in Figure 2.1. The influence of the GSC is neglected by having CB5 open and CB4 closed so that the GSC can freely regulate the converter dc-link voltage. Opening CB1 to disconnect from the utility when CB3 is closed to power a local load induces turbine load transient which is measured at the stator MGT. Frequency and voltage at load 2 is then completely dependent on wind turbine response. This response is examined in Figure 2.11 for several control sets in Table 2.2. Before and during transient, load 2 draws 6.1 kW; 56 % more power than provided by the turbine in steady-state with MPPT at 1544 rpm, 3.9 kW.

Table 2.2 Control designs providing TQ and FV response

Design:	B	C	D	E	F	G	H	I
τ_2 (s)	0.16	0.16	0.16	0.16	0.16	0.16	0.16	0.16
$s_{p\,T,Q}$ (rad/s)	-0.5	-0.5	-0.5	-0.5	-0.5	-0.5	-0.5	-0.5
$s_{z\,T,Q}$ (rad/s)	-0.3,-1	-0.3,-1	-0.3,-1	-0.3,-1	-0.3,-1	-0.3,-1	-0.3,-1	-0.3,-1
τ_3 (s)	0.08	0.08	0.08	0.08	0.08	0.08	0.08	0.08
$s_{p\,F,V}$ (rad/s)	-10	-10	-10	-10,-1	-1,-0.1	-20,-1	-20,-10	-40,-10
$s_{z\,F,V}$ (rad/s)	-20	-20	-20	-100,-2	-10,-0.2	-200,-2	-200,-	-400,-
τ_4 (s)	15	15	15	15	15	15	15	15
τ_6 (s)	10	5	2	5	5	5	5	5
$\Delta f_{e,\ \text{nadir}}$	0.0028	0.0041	0.035	0.55	6.35	0.16	0.23	0.34
t_{nadir} (s)	0.13	0.99	0.79	0.33	1.94	0.51	0.22	0.26
$f_{e,\,t=0.2\,s}$ (Hz)	60.0	60.0	60.0	59.6	59.5	59.8	59.8	59.7

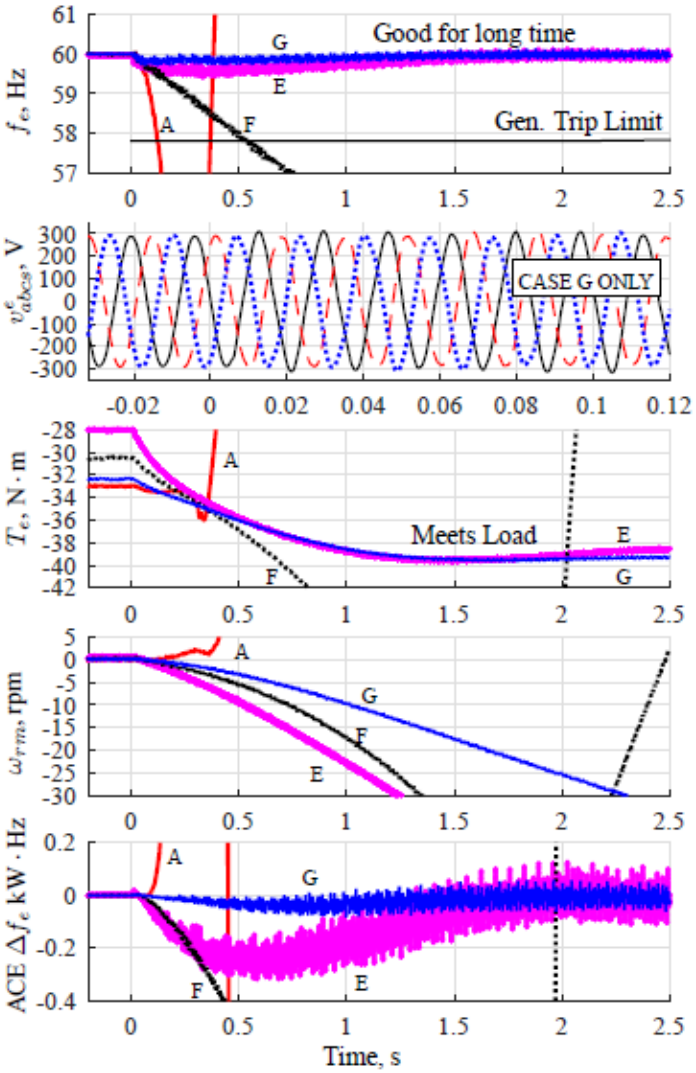

Figure 2.11 Experimental response to utility loss, imposing 100 % dependence of load on DFIG wind turbine inertial response. Stator voltage of Case D is zoomed to the first 100 ms after transient onset; it is maintained nicely as rotor speed drops with support of the load.

Relative pole and zero placement effects the peak inertial torque and response damping. TQ-only control of case A is clearly unstable. Slow control of case F is still unstable yet with improvement from A. Faster FV control (cases E & G) result in stronger load support and thus higher frequency nadir. Frequency and voltage transients are sufficiently arrested and inertial response is sustained into the primary frequency control range.

Islanding response under two loading conditions and two control designs are in Figure 2.12. Design H is tested with load $1.1P_{s,\,MPPT}$ and $1.6P_{s,\,MPPT}$. For the larger, frequency nadir drops only 230 mHz at 220 ms, and stays above 59.6 Hz for longer than 15 s. With a load of $2.7P_{s,\,MPPT}$ (that's $1.4P_{rated}$), design I is able to maintain frequency for more than six seconds. Even with large overload stator frequency is held within generator protection limits and over/under frequency load shedding limits while the rotor accelerates in response.

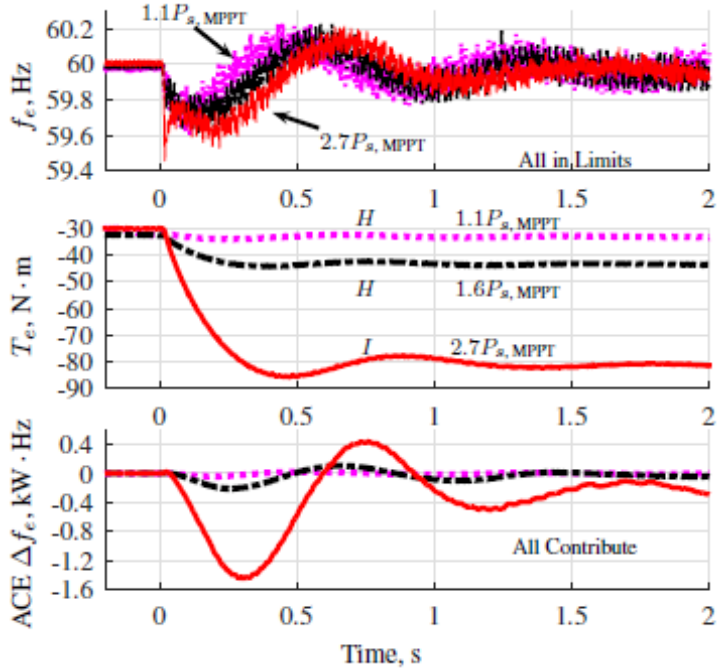

Figure 2.12 Open-utility islanding response, subjecting the DFIG to small and large overload conditions.

The controller automatically adusts generator torque to satisfy the load demand. ACE$\Delta f_e < 0$ is the evidence of supportive response. Frequency response is specified by controller pole/zero placement.

2.3.3 Islanding response when including GSC influence:

Earlier sections have shown significant frequency response capability via stator-coupling to the rotor mass, and a control architecture was proposed to link rotor kinetic energy to the electrical frequency response. To study the DFIG capability as commonly configured today, we perform tests with the GSC controlling the dc-link and connected to the stator by CB5, with CB4 open. Energy cannot be sourced from anywhere except the physical rotor.

Since the GSC handles only up to one-third of the total power in steady-state, and because it is designed to follow applied voltage, its influence is not expected to be great. Although, operation at sub-synchronous rotor speeds requires power be injected into the rotor terminals by the MSC. So in response to additional stator load requirement then, the MSC will draw energy from the dc-link and thus the GSC which may degrade the frequency response. The operation at super-synchronous speeds requires the MSC extract real power from the MCT, so when additional power is needed to support increased stator load, the MSC will effectively make the GSC reduce the amount of power it is delivering to the load at the MGT in exchange for its use in frequency response via the MSC; response is not expected to change much in this condition. Results of islanding response under these conditions is provided in Figure 2.13.

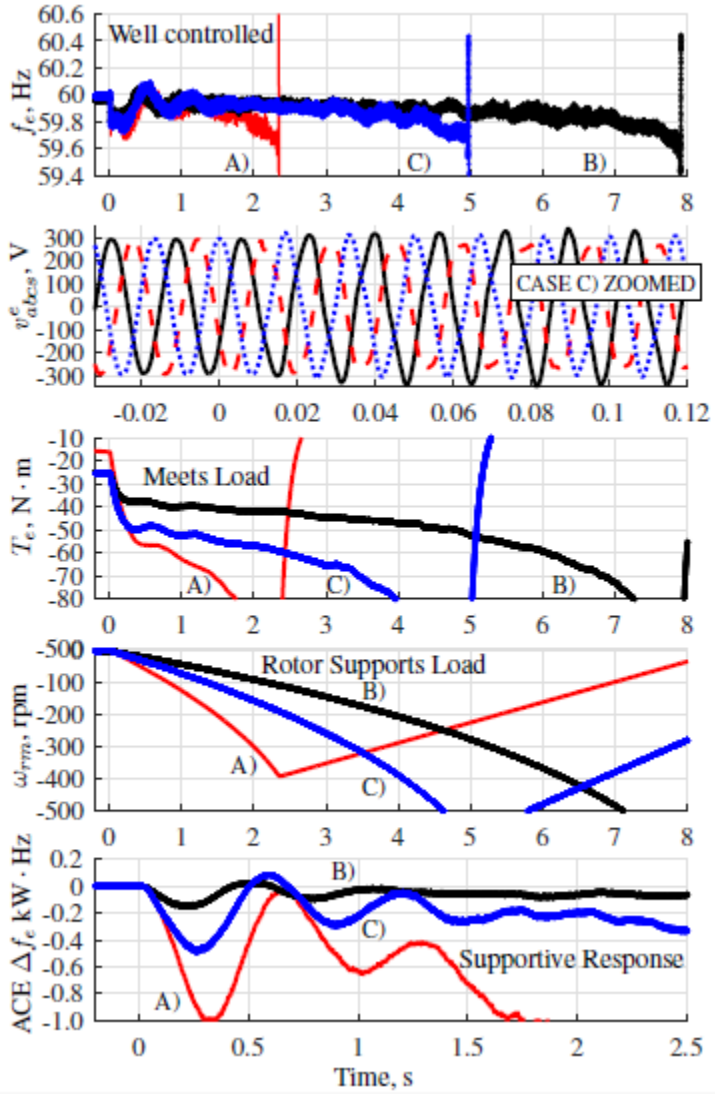

Figure 2.13 Islanding frequency response with the GSC connected at the stator terminals. Shown is response when A) $\omega_{rm} < \omega_{sync}$ with CB2 closed and load 1 drawing $2.4P_{MPPT}$, and also at $\omega_{rm} > \omega_{sync}$ with B) CB2 closed drawing $1.17P_{MPPT}$ and C) CB3 closed drawing $1.41P_{MPPT}$.

Each case in Figure 2.13 has the same controller design; FV poles placed at -20 rad/s, TQ poles at -0.5 rad/s, and the HPF corner frequency at 2 Hz. Notice that for all three, the frequency response has similar appearance – a matter of transfer function design. Inertial current commands increase the generator torque in effort to maintain frequency. As time goes on without primary response, the frequency command via the LPF continues to decline and torque is further increased until the DFIG faults due to rotor over-current. Supportive response is provided by the rotor mass, evidenced by ACE$\Delta f_e < 0$; stator voltage is also maintained with good quality.

2.4 Conclusions of adding a frequency-responsive controller

DFIG wind turbines do contribute to frequency response, but controls in use today can hinder those efforts. The DFIG controller we propose counteracts those harmful effects. It requires no headroom, additional hardware, or communication and is easy to design. The method contributes rotor kinetic energy to support load change, not simply frequency change. Temporary inertial excursion allows return to normal MPPT operation. We have proven exceptional frequency response even under extreme islanding conditions. The proposed controller complements existing generator controls and is beneficial to utility operation. We've added a valuable service to DFIG wind turbines that affords response flexibility and performance previously not achieved. This project has derived the relationship between frequency stability and generator control for low-inertia conditions. It has provided a mathematical basis and experimental proof to support claims of frequency support capability. We applied the proposed inertial frequency controller in high and low-inertia systems, under light and heavy loading conditions, and with a range of control tuning scenarios. Compared to the existing state of art, we have achieved superior frequency response.

3. DFIG Reactive Power Capability

The ability for DFIG wind turbines to provide reactive power generation is critical for reliable grid operation and enhancing their capability adds value to the resource. Added reactive power capability can improve low-voltage transient response [34]. A recent discovery of configuring the DFIG with a grid-connected rotor winding is inverse to the normal method but has shown to result in improved efficiency due to reduced core loss [33]. This configuration is also shown to utilize the generator material more effectively [35]. In this section we derive the DFIG reactive power capability on a mathematical basis and propose the rotor-tied configuration to enhance generation capability. Candidate machines are studied with improvements observed. This shows the ability for DFIG wind turbines to meet RTE requirement for providing $0.3P_{n\ rated}$ var capability.

The primary challenge is to provide reactive generation capability. Wind turbines with squirrel-cage induction generators offer no control and actually consume reactive power. Motor loads consume reactive power and power electronic loads with unity power factor do not support added inductive or capacitive load. The objectives of this project are to understand the DFIG capability and to propose a method to enhance low-voltage support effects. Goals are achieved through careful analysis of power converter and generator capability and nameplate specifications with enhancement achieved from more effective application of the power converter by connecting it to the DFIG terminal having the highest current and lowest voltage rating. Specific objectives of this section are to:

1. Propose the rotor-tied configuration for increased reactive power generation.
2. Derive expressions to evaluate reactive power generation capability in the stator-tied configuration (STC) and rotor-tied configuration (RTC).
3. Quantify impact of proposed RTC on a surveyed range of wind turbine generators.

Subsequently, the reactive power capability boundaries are formulated. Case studies are performed with a range of small to MW-size machines. Laboratory experiments of one machine validate expectations and illustrate potential benefit of the RTC.

3.1 Modeling reactive power capability

The DFIG wind turbine is normally connected to the power system via a direct stator-to-grid connection through a circuit breaker and with the rotor terminal connected via a back-to-back converter that controls power flow, torque and reactive power, through the machine, as illustrated in Fig. 3.1. A series reactor may be used between machine-side converter (MSC) and the converter-side terminal (CST) to limit converter current ripple. Power is defined positive for current injected into the machine; negative value implies generation from the machine.

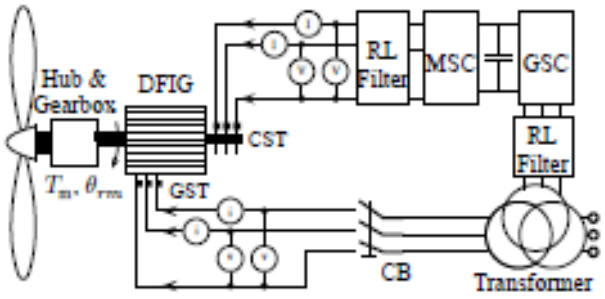

Figure 3.1 High-level model of the DFIG wind turbine with back-to-back power converter.

Mechanical shaft power is defined by the controller according to incoming wind speed to achieve maximum power extraction

$$P_m = -0.5\rho C_p A v_{wind}^3 \, . \tag{3.1}$$

Real power at rotor and stator terminals, P_r and P_s, are related to the mechanical shaft power according to slip, s, by

$$P_s = \frac{P_m}{1-s} \tag{3.2}$$

$$P_r = -sP_s, \tag{3.3}$$

where slip is $s = (\omega_e - \omega_r)/\omega_e$. For generator action, $P_m = T_m\omega_{rm} > 0$, where T_m is shaft torque due to wind and ω_{rm} is the mechanical rotor speed. To limit converter power rating to one third of the total power the P-pole generator has electrical rotor speed, $\omega_r = P/2\omega_{rm}$, refined to $|\omega_r| = \{\pi f_{grid}, 3\pi f_{grid}\}$. Since rotor and stator electrical frequency are related by slip so that $f_r = sf_s$ then the converter frequency is limited to only 30 Hz max and which can correspond to the wind speed range of 4-12 m/s.

The DFIG is modeled using a T-equivalent per-phase steady-state circuit as drawn in Fig. 3.2. Applying a grid voltage according to nameplate value and assuming a real-power condition according to maximum power point tracking of a wind turbine, the circuit can be solved for a range of stator or rotor terminal reactive power values. The corresponding current magnitude shall be limited to nameplate value, thus providing bounds on the reactive power capability.

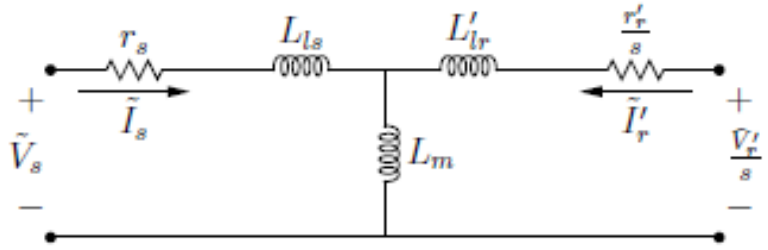

Figure 3.2 Per-phase T-Equivalent steady-state circuit model of the DFIG wind turbine. Note: not shown are filter elements between the MSC and the CST.

Estimation of the reactive power capability boundaries is formulated using phasor notation and the concept of available apparent power. Before equating bounds of the reactive power region it is useful and interesting to understand the reactive power requirement of the generator itself. The MSC has capability to generate or consume reactive power but the demand at the grid terminal also depends on consumption created by DFIG inductance. Some voltage is dropped across leakage inductance parameters L_{ls} and $L_{lr}^{'}$ and a relatively larger portion of reactive current is required to magnetize the core represented by inductance L_m. Reactive power consumed by the machine is estimated for magnetization by either the stator (subscript STC) or rotor (subscript RTC) as:

$$Q_{m,\mathrm{RTC}} \sim \frac{3}{2}\frac{s\,V_{r,\mathrm{grid}}'^{\,2}}{2\pi f_{\mathrm{grid}} L_r'} \tag{3.4}$$

$$Q_{m,\mathrm{STC}} \sim \frac{3}{2}\frac{s\,V_{s,\mathrm{grid}}^{2}}{2\pi f_{\mathrm{grid}} L_s}, \tag{3.5}$$

where generator inductances are combined as $L_r^{'} = L_m + L_{lr}^{'}$ and $L_s = L_m + L_{ls}$. Notice that relative difference in the values of $L_r^{'}$ and L_s leads to difference in the reactive power consumption of the generator. Votlage V_s or $V_r^{'}/s$ have identical value when applied at nameplate rating and after referral of rotor quantities to the stator via the turns ratio. Leakage inductance influences the core consumption and thus grid-terminal capability.

Reactive power at the generator GST is exchanged via the MSC. Slip, *s*, amplifies reactive power coupling of stator and rotor terminals. At synchronous rotor speed the MSC provides zero reactive power since the converter current is dc. Away from synchronous speed the MSC reactive power is increased to maintain value at the GST. Amplification of reactive power across the machine is quantified by considering the steady-state terminal voltage.

$$\tilde{V}_s = \tilde{I}_s r_s + j\omega_e L_s \tilde{I}_s + j\omega_e L_m \tilde{I}_r' \tag{3.6}$$

$$\tilde{V}_r' = \tilde{I}_r' r_r' + j\omega_e L_r' \tilde{I}_r' + j\omega_e L_m \tilde{I}_s. \tag{3.7}$$

Apparent power at a terminal is $S = 3\tilde{V}\tilde{I}^{*}$, so

$$Q_s = 3\,Im\{r_s \tilde{I}_s^2 + j\omega_e L_s \tilde{I}_s^2 + j\omega_e L_m \tilde{I}_r' \tilde{I}_s^{*}\} \tag{3.8}$$

$$Q_r = 3\,Im\{r_r' \tilde{I}_r'^2 + j\omega_e L_r' \tilde{I}_r'^2 + j\omega_e L_m \tilde{I}_s \tilde{I}_r'^{*}\}. \tag{3.9}$$

The first term is purely real, so this becomes

$$Q_s = 3\omega_e L_s \tilde{I}_s^2 + 3\,Im\{j\omega_e L_m \tilde{I}_r' \tilde{I}_s^{*}\} \tag{3.10}$$

$$Q_r = 3\omega_e L_r' \tilde{I}_r'^2 - s3\,Im\{j\omega_e L_m \tilde{I}_s^{*} \tilde{I}_r'\}. \tag{3.11}$$

Equating the last term of (3.10) and (3.11) while neglecting leakage inductance yields

$$\frac{Q_r}{s} = 3\omega_e L_m (\tilde{I}_r'^2 + \tilde{I}_s^2) - Q_s \tag{3.12}$$

and shows how slip amplifies terminal reactive power and how stator and rotor current magnitude influence reactive power flow between terminals.

Nameplate current rating of generator and MSC must not be exceeded. It is assumed that the power converter is rated to a larger current magnitude than the generator terminal it is connected to. Generator nameplate current is a limiting factor in reactive power capability. A portion of the current capacity must be used for real power exchange. Total real power is assumed in accordance with (3.1) and is split between rotor and stator terminals according to (3.2) and (3.3). Then the reactive power limitation due to nameplate current rating and generator magnetizing inductance can be derived.

Considering the conventional STC and the stator current limit, apparent power at the GST is

$$S_s = P_s + jQ_s = 3\tilde{V}_s\tilde{I}_s^*.$$

$$\frac{P_m}{1-s} + jQ_s = 3V_s\mathrm{Re}\{\tilde{I}_s\} - j3V_s\mathrm{Im}\{\tilde{I}_s\}. \tag{3.13}$$

The real and reactive stator current is then

$$\mathrm{Re}\{\tilde{I}_s\} = \frac{P_m}{(1-s)3V_s} \tag{3.14}$$

$$\mathrm{Im}\{\tilde{I}_s\} = \frac{-Q_s}{3V_s}. \tag{3.15}$$

The maximum allowed stator current is $I_{s,rated} = \sqrt{(\mathrm{Re}\{\tilde{I}_s\})^2 + (\mathrm{Im}\{\tilde{I}_s\}_{max})^2}$, so

$$Q_{s,I_{s,rated}} = -3V_s\mathrm{Im}\{\tilde{I}_s\}_{max} \tag{3.16}$$

$$Q_{s,I_{s,rated}} = -3V_s\sqrt{I_{s,rated}^2 - (\mathrm{Re}\{\tilde{I}_s\})^2} \tag{3.17}$$

$$Q_{s,I_{s,rated}} = -3V_s\sqrt{I_{s,rated}^2 - \frac{P_m^2}{9(1-s)^2V_s^2}}. \tag{3.18}$$

Equation (3.18) can be plotted against wind speed. This boundary is a circular arc.

Rotor current rating places another bound on reactive power capability. A similar process as (3.13) – (3.18) is used to consider the rotor current limit in the conventional STC. Stator real and reactive power are written in terms of stator voltage and rotor current as:

$$P_s = -3\frac{L_m}{L_s}V_sI_r'\cos(\theta) \tag{3.19}$$

$$Q_s = 3\frac{V_s^2}{L_m\omega_e} - 3\frac{L_m}{L_s}V_sI_r'\sin(\theta), \tag{3.20}$$

where θ is the angle between the stator voltage and the rotor current. At rated rotor current

$$P_r = 3s\frac{L_m}{L_s}V_s I'_{r,rated}\cos(\theta) \tag{3.21}$$

$$Q_{s,I_{s,rated}} = 3\frac{V_s^2}{L_m\omega_e} - 3\frac{L_m}{L_s}V_s I'_{r,rated}\sin(\theta), \tag{3.22}$$

so

$$\frac{-sP_m}{(1-s)} = 3s\frac{L_m}{L_s}V_s I'_{r,rated}\cos(\theta) \tag{3.23}$$

$$Q_{s,I'_{r,rated}} = 3\frac{V_s^2}{L_m\omega_e} - 3\frac{L_m}{L_s}V_s I'_{r,rated}\sin(\theta). \tag{3.24}$$

Rearranging (3.33) and (3.34) leads to

$$\theta = \text{acos}\left(\frac{-P_m L_s}{3(1-s)L_m V_s I'_{r,rated}}\right) \tag{3.25}$$

$$Q_{s,I'_{r,rated}} = 3\frac{V_s^2}{L_m\omega_e} - 3\frac{L_m}{L_s}V_s I'_{r,rated}\sin\left(\text{acos}\left(\frac{-P_m L_s}{3(1-s)L_m V_s I'_{r,rated}}\right)\right). \tag{3.26}$$

Equation (3.26) can be plotted against wind speed via slip. At cut-in speed s = 0.5 and the boundary takes the shape of nearly a line. $I'_{r,rated}$ can be taken to have positve value; making it have negative value provides another possible boundary made by the rotor current magnitude limitation.

Formulas of (3.18) and (3.26) provide basis for evaluating reactive power capability limits when operating in the STC. They will be used in a later section for specific case studies.

3.2 Proposed RTC to shift reactive power capability toward generation

We can enhance the reactive power generation capability in certain generators by applying them with an alternative connection strategy. We propose a configuration that is inverse to convention, in which the rotor windings are connected to the grid and the power converter is connected to the stator windings. The proposed RTC and conventional STC are drawn in Fig. 3.3.

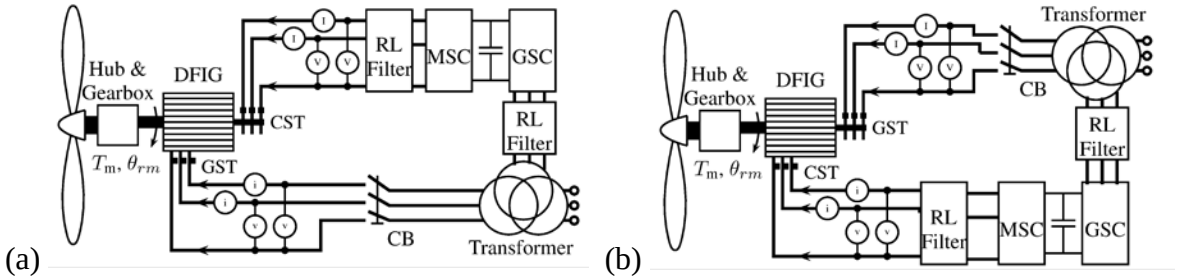

Figure 3.3 Conventional (a) and proposed (b) connection strategy for the DFIG wind turbine.

For both STC and RTC the same definition of slip applies, $s = (\omega_e - \omega_r)/\omega_e$, where ω_e is the electrical stator frequency and $(\omega_e - \omega_r)$ is the frequency of rotor current. Hence, by (3.2) and (3.3) the power converter handles 1/3 of total mechanical power P_m.

In the RTC, the grid must be connected to the rotor terminal with a negative sequence. In this way the rotor is defined to have $\omega_r < 0$. The rotor current now has grid-frequency, i.e. 60 Hz, and the converter (stator) frequency is $\omega_e = 2\pi f_{\text{grid}} + \omega_r$ and lies in the range {-30, 30} Hz. The useful slip range of the RTC is illustrated in Figure 3.4. Notice the slip at synchronous speed is $|s| = \infty$, equivalent to the STC condition where $|s| = 0$ at synchronous speed. Generator electrical parameters are also valid in both STC and RTC.

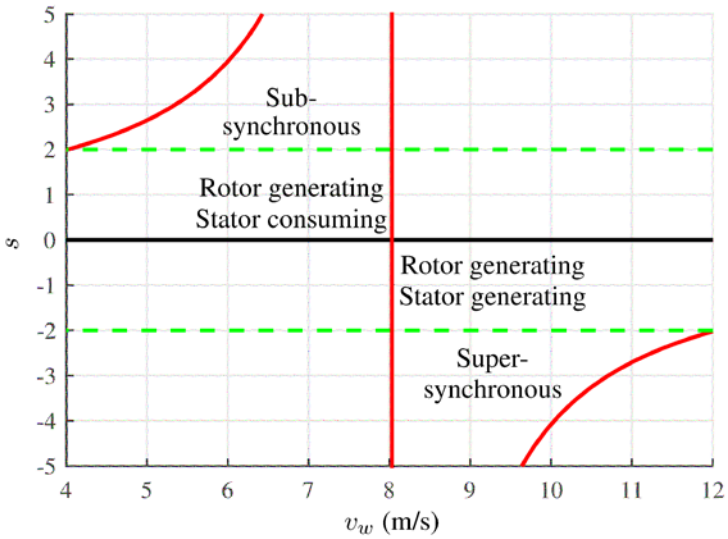

Figure 3.4 Sip curve in the RTC. Notice the asymptote at synchronous speed.

Reactive power at the GST in the RTC is formulated in a way similar to that done previously for the STC. To consider the generator nameplate rotor current rating, rotor apparent power is written as

$$S_r = P_r + jQ_r = 3\tilde{V}_r'\tilde{I}_r'^{*} \tag{3.27}$$

$$\frac{sP_m}{(1-s)} + jQ_r = 3V_r'\text{Re}\{\tilde{I}_r'\} - j3V_r'\text{Im}\{I_r'\}, \tag{3.28}$$

while keeping in mind that $P_m < 0$ for generation. Real and reactive rotor currents are therefore

$$\text{Re}\{\tilde{I}_r'\} = \frac{sP_m}{(1-s)3V_r'} \tag{3.29}$$

$$\text{Im}\{\tilde{I}_r'\} = \frac{-Q_r}{3V_r'}. \tag{3.30}$$

The maximum allowed rotor current is related using $I'_{r,\text{rated}} = \sqrt{(\text{Re}\{\tilde{I}_r'\})^2 + (\text{Im}\{\tilde{I}_r'\}_{\max})^2}$, so

$$Q_{r,I'_{r,\text{rated}}} = -3V_r'\sqrt{I'^2_{r,\text{rated}} - \frac{s^2P_m^2}{9(1-s)^2V_r'^2}}. \tag{3.31}$$

Equation (3.31) forms a bound that takes shape as a circular arc and is easily plotted with wind speed.

The stator current limit in the RTC is considered by arranging rotor reactive power in terms of rotor voltage and stator current, as

$$Q_{r,I_{s,\text{rated}}} = 3\frac{V_r'^2}{L_m\omega_e} - 3\frac{L_m}{L_r'}V_r' I_{s,\text{rated}}\sin(\theta), \tag{3.32}$$

where θ is the angle between rotor grid voltage and stator converter current. Angle θ is related using power and slip, so using (3.2)

$$\frac{\mathrm{P_m}}{(1-\mathrm{s})} = 3\frac{\mathrm{L_m}}{\mathrm{L_r'}\mathrm{s}}\mathrm{V_r'}\mathrm{I_{s,rated}}\cos(\theta) \tag{3.33}$$

$$\theta = \mathrm{acos}\left(\frac{\mathrm{sP_m L_r'}}{3(1-\mathrm{s})\mathrm{L_m V_r' I_{s,rated}}}\right). \tag{3.34}$$

Reactive power can be pushed or pulled through the machine until either rotor or stator current limit of (3.31) or (3.32), respectively, is reached.

3.3 Case studies of Reactive Power Capability

We apply theoretical bounds of reactive power capability in case study of specific machines. A 10 Hp DFIG resides in the WESL at ISU. We perform experiments on that machine and observation concurs with expectation, validating formulations of (3.22), (3.24), (3.26), (3.31), and (3.32). Another DFIG we consider is a 150 W machine that also resides at the WESL. We study a 2 MW DFIG and show evidence that concurs with RTE's expected performance requirements but is discrepant with manufacturer stated capability and field observation. One objective of this study is to provide the theoretical basis for the expected capability. A possible cause for that machine's field-observation of diminished reactive power generation capability is also provided; excessive MSC filter inductance and limited efficiency may be factors. We also study a set of DFIGs that have electrical parameters available in existing literature using circuit analysis in STC and RTC. Some of those are shown to have reactive power generation enhancement due to improved efficiency and thus added current headroom when in the RTC.

3.3.1 Experiments with a 10 Hp laboratory DFIG

A 10 Hp DFIG is studied considering its electrical parameters and nameplate voltage and current ratings, which are available in [33]. Boundaries of reactive power capability are plotted by (3.22) – (3.26) and (3.31) – (3.34) in Figure 3.5. A cut-in wind speed of 4 m/s is considered according to the specified gear ratio, tip-speed ratio, rotor speed range, and slip range. For this machine the limiting bounds in the STC are (3.24) for reactive power generation and (3.18) for consumption. For the RTC the limiting bounds are (3.31) for generation and (3.32) for consumption.

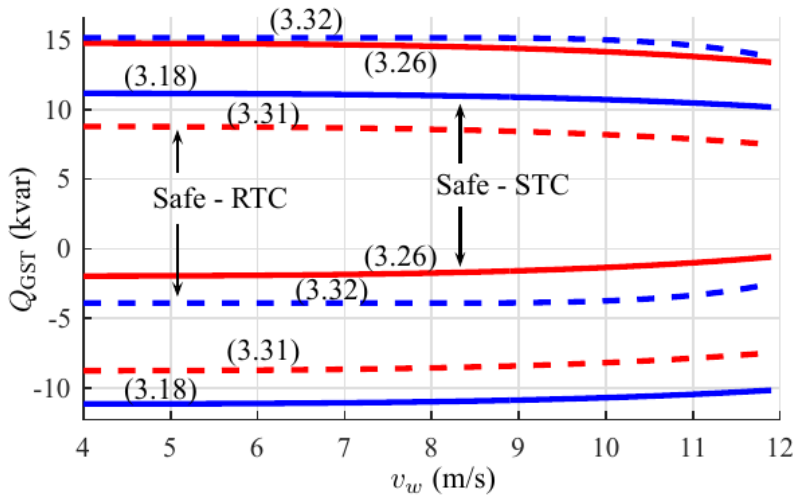

Figure 3.5 Boundaries of the GST reactive power capability.

The per-phase equivalent circuit solved for range of GST reactive power and corresponding real power for MPPT over the wind speed range. The GST and corresponding CST reactive power regions are plotted in Figure 3.6.

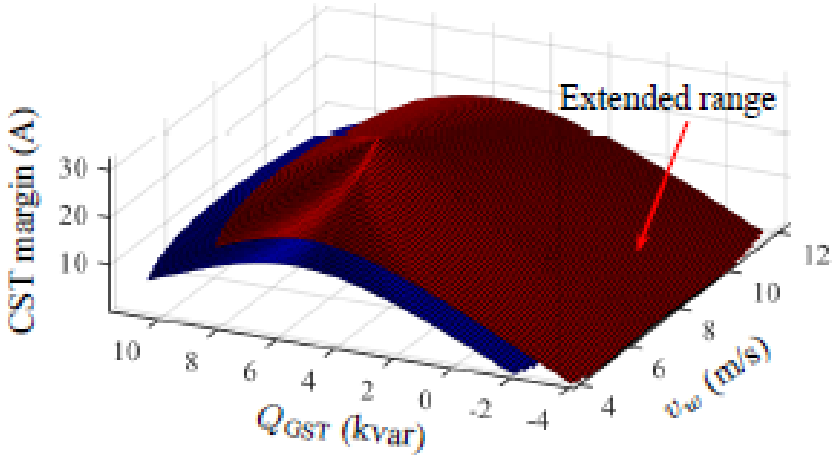

Figure 3.6 Reactive power operating region at the GST and CST over the wind speed range.

The shift of frequencies within the machine cause a clear shift of the GST reactive power operating region toward ability for generation. The shift is caused by the difference of rotor and stator leakage inductance and alternate rotor and stator nameplate current rating. This is observed in Figure 3.7 by difference in the CST current margin over the region. The result is expected according to (3.10) – (3.12). Efficiency advantage gained in the RTC is also observed via the steady-state analysis. The shift of real and reactive power region observing the efficiency gain is plotted in Figure 3.7. Notice this machine has poor efficiency at low wind speed, yet can still produce reactive power.

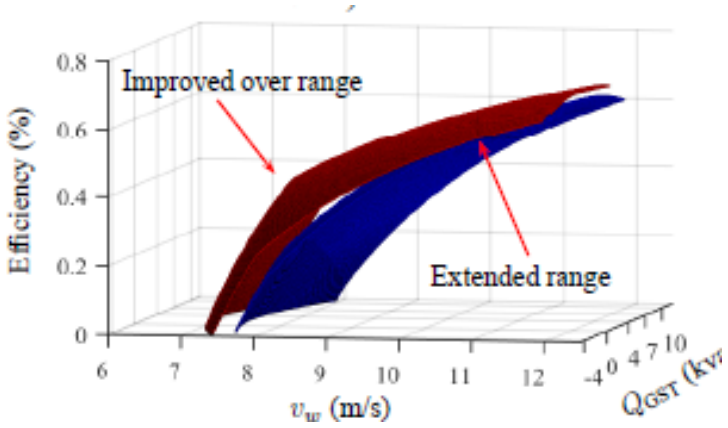

Figure 3.7 Efficiency improvement in the RTC adds current headroom for reactive capability.

Bounds observed in the 3-dimensional operating region consider resistive loss as well as hysteresis core loss using the method in [36]. The bounds are slightly different than estimated with (3.22) – (3.26) and (3.31) – (3.34) but agree well with the general trend. The bounds of the 3D region are drawn in Figure 3.8.

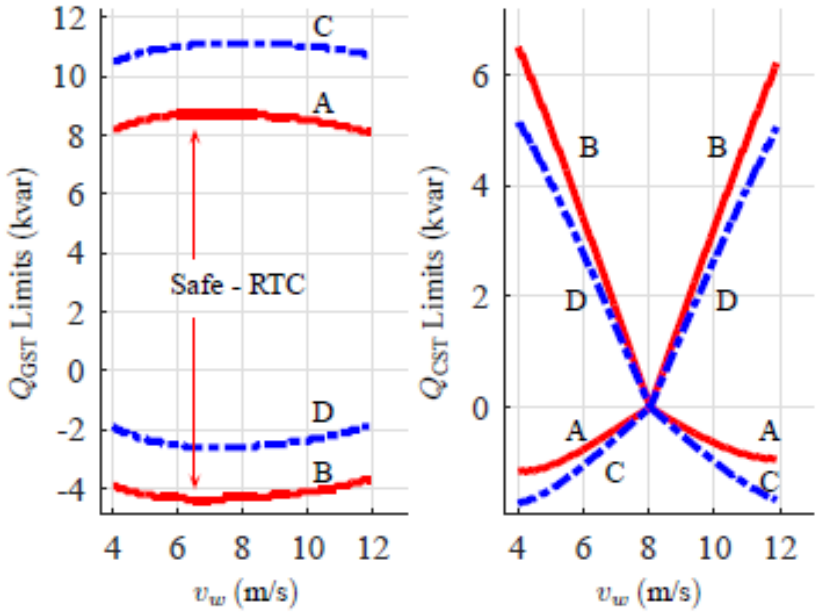

Figure 3.8 Bounds of GST reactive power capability and corresponding CST reactive power.

This machine is expected to experience nearly double the reactive power generation capability when in the RTC. The STC may be preferred for reactive power consumption capability. Experiments performed in both STC and RTC validate the enhanced capability. The GST reactive power is plotted with corresponding converter reactive power in Figure 3.9. The CST reactive power is expected by the approximate association described by (3.12).

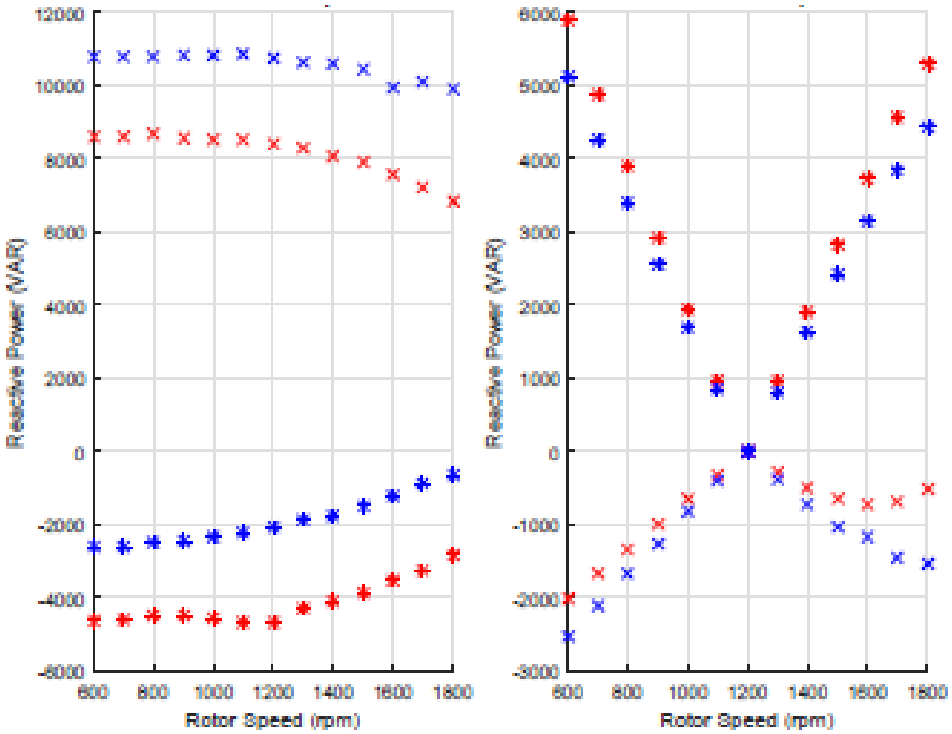

Figure 3.9 Reactive power capability at (a) the GST and (b) CST for the RTC (red) and STC (blue). *Note:* 'x' and '*' points correspond between plots.

The laboratory DFIG is shown here to experience enhanced reactive power generation capability when applied in the RTC. Efficiency improvement is also observed. Depending on specific ancillary service objectives of this machine, the RTC may be preferred. These experiments validate theoretical expectations derived earlier in this section.

3.3.2 RePower MM82 2.0 MW

The RePower MM82 2.05 MW wind turbine uses a DFIG. The generator is manufactured by VEM as model DASAA 5025-4UA [30]. Actual and theoretical reactive power capability can vary by causes of turbine design and control. This section applies the formulations developed here to calculate and analyze the reactive power boundaries of this generator.

Discrepancy of stated, observed, and third-party study is summarized in [31] and sketched in Figure 3.10. The first revision of the generator and turbine design had manufacturer capability indicated by the green line and labeled "2007". A second revision of the system lead to capability indicated by the red line and labeled "2012". Both indicate diminished capability at low wind speed and low real power.

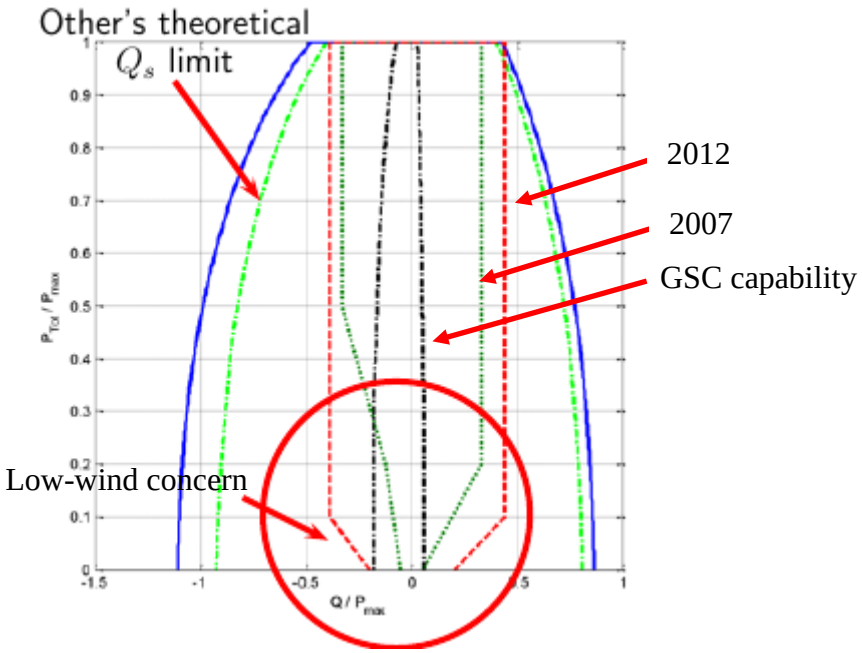

Figure 3.10 Comparison of specified and expected GST reactive power capability. *Note:* GSC reactive power capability is also plotted here.

Applying equations (3.22) – (3.26) and (3.31) – (3.34) provides insight to the theoretical capability when considering the generator electrical parameters and nameplate capacity. Parameters and capacity are listed as V_s = 690 V, V_r = 1620 V, I_s = 1586 A, I_r = 808 A, P = 4, g = 120, λ = 6.5, f = 50 Hz, L_m = 2.8 mH, L_{ls} = 94.8 µH, L_{lr}' = 62.4 µH, R_s = 1.6 mΩ, and R_r' = 1.49 mΩ. The converter dc-link voltage is 1100 V. For the slip range of this turbine, s = [0.4,-0.2], the converter voltage is sufficient to provide the reactive power requirement. Approximate boundaries of GST reactive power capability of (3.22) and (3.24) is plotted in Figure 3.11, assuming the conventional STC. The dot-dash line indicates boundary due to stator current limit and the dash-dash line indicates the boundary due to the rotor current limit.

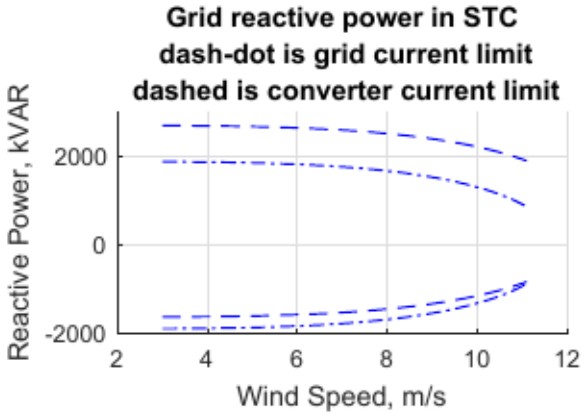

Figure 3.11 Approximate boundaries of reactive capability at rotor and stator current limits.

For both reactive power generation and consumption at the GST, the stator current rating is the limiting factor. Generator parameters and nameplate ratings indicate the generator is capable of producing even more reactive power than RTE requires.

Considering possible benefit from operating in the RTC, equations (3.31) – (3.34) are applied and plotted in Figure 3.12. Again the limiting factor is the grid-side current. Note that operation in this condition would require a converter modification to operate with the larger voltage and lower current specified for a stator-connected converter. The grid-coupling transformer would also need reconsideration. Cost benefit analysis to consider design modifications and to analyze preference is not provided but could provide useful future insight.

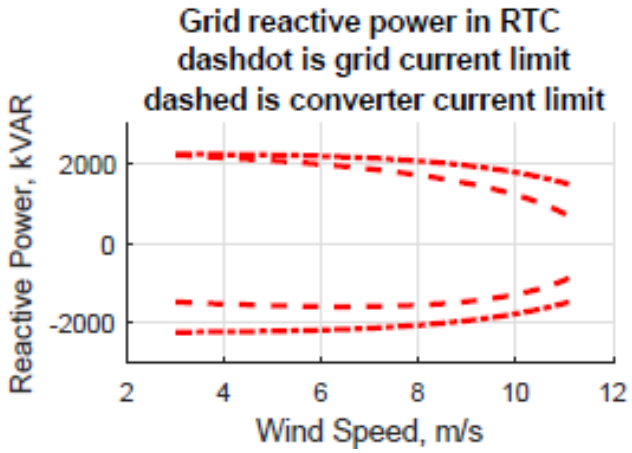

Figure 3.12 GST reactive power capability when in the RTC; note similarity to the STC.

Full circuit analysis provides further insight considering also core and ohmic loss. Machine-grid terminal (MGT) and machine-converter terminal (MCT) reactive power boundaries in both STC (blue, dashed) and RTC (red, solid) are drawn in Figure 3.13. When a high-voltage converter is allowed for use with the RTC, both configurations offer sufficient and competitive capability.

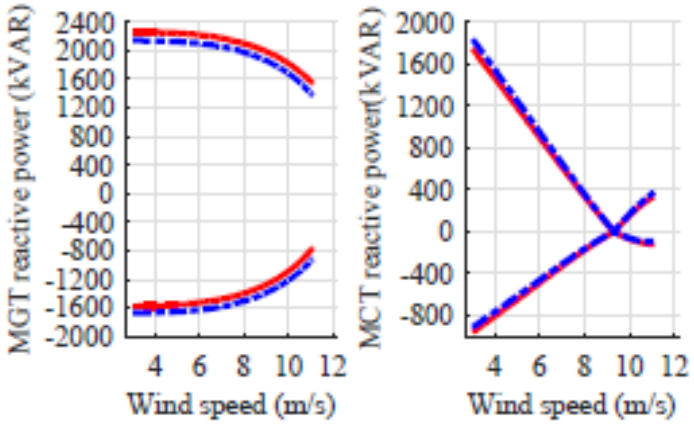

Figure 3.13 Comparison of reactive power capability in both the STC and the RTC.

A point to consider is that generator efficiency drops substantially when exchanging large quantities of reactive power, no matter the configuration. Plotted in Figure 3.14 is the efficiency

over the total real and reactive power operating region, for the RTC (red) and STC (blue). Notice the RTC is more efficient. Also, if the RTC employs a modified transformer and converter to match the generator nameplate, the reactive power capabilities are competitive as well. Further study of cost and benefit would be required to identify a preferred configuration.

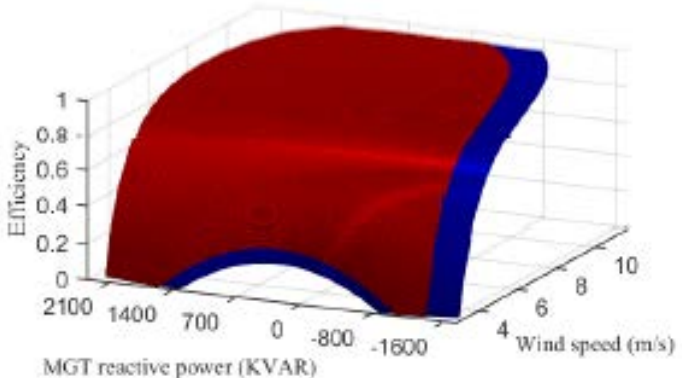

Figure 3.14 Efficiency of the DFIG wind turbine in RTC (red) and STC (blue) over the entire real and reactive operating region.

Notice in Figure 3.14 that at low wind speed the efficiency drops below zero. Limiting operation to avoid net loss via control functions may be an explanation for diminished reactive capability at low wind speed.

This section has shown that the VEM DASAA 5025-4UA has sufficient capability to meet the RTE system requirement of $0.3P_{n,\text{rated}}$ and has provided possible explanation for observing diminished capability at low wind speed.

3.3.3 Other machines of interest

Additional DFIGs have been studied to identify candidates for possible reactive power generation enhancement when in the RTC. These machines have electrical parameters available in existing literature. Some references do not list the rotor nameplate voltage and current ratings and so those machines are assumed here to have equal stator and voltage rating. Shift of reactive power capability is estimated considering only added current headroom due to efficiency improvement. Solutions based on the equivalent steady-state circuit are provided for each machine in Table 3.1.

Table 3.1 Reactive power generation increase for surveyed DFIGs.

Machine	1 [37]	2 [33]	3 [38]	4 [39]	5 [40], [41]	6 [42]	7 [43]	8 [43]
P_{ratred} (kw)	0.15	7.5	1700	1500	2000	2000	1500	1000
$V_{s,\text{rated}}$ (V)	120	208	690	575	690	690	690	575
$V_{r,\text{rated}}$ (V)	60	195	690	575	690	690	690	575
$I_{s,\text{rated}}$ (A)	1.5	31	1600	1600	1600	1600	1600	1600
$I_{r,\text{rated}}$ (A)	2	26	1600	1600	1600	1600	1600	1600

f_{rated} (Hz)	60	60	50	60	50	50	50	60
P	4	6	4	6	4	4	4	4
R_s (mΩ)	12183	143.4	1.615	1.565	2.199	1.164	2.650	3.654
L_{ls} (mΩ)	55.89	2.137	0.092	0.100	0.120	0.070	0.1687	0.1304
R_r' (mΩ)	13105	95.57	2.369	1.102	1.799	1.310	2.630	3.569
L_{lr}' (mH)	55.89	1.75	0.082	0.091	0.050	0.075	0.1337	0.1198
L_m (mH)	404.5	17.93	2.508	1.696	2.90	2.995	5.475	4.12
r_a (m)	0.055	0.055	0.55	0.50	0.60	0.60	0.50	0.35
l (m)	0.08	0.26	1.55	1.50	1.60	1.60	1.50	1.35
$\Delta Q_{\text{GST gen, cut-in}}$ (%)	400	105.3	0	0	2.26	-0.73	0.63	0.75
$\Delta Q_{\text{GST gen, sync}}$ (%)	-67.8	50	5.88	6.32	9.68	6.25	3.92	2.29
$\Delta Q_{\text{GST gen, cut-out}}$ (%)	350	94.7	1.14	0	6.41	-1.20	0.77	0

Generation enhancement is observed for most machines, but for others benefit varies. For machine 1, reactive generation is improved in the RTC at high and low wind speed, but diminished at synchronous speed. Machine 6 has an opposite effect. Variation of performance enhancement is illustrated for machine 1 in Figure 3.15.

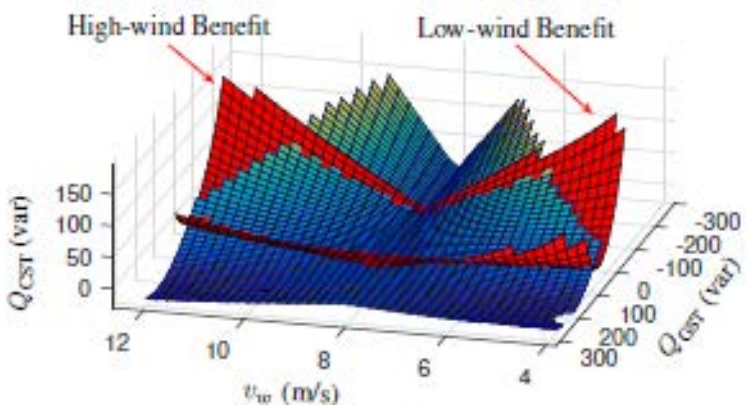

Figure 3.15 Reactive power capability of this machine is enhanced at high and low wind speed when in the RTC (red). The STC (blue) has better generation capability at synchronous speed.

The RTC provides an option to consider when designing wind turbines that use DFIG technology. Preference of STC or RTC may vary depending on the specific generator and the intended ancillary service objectives. Careful consideration of both DFIG configurations can lead to improved utility of wind turbine generators.

4. Conclusions

This project has investigated frequency and reactive power support capabilities of power electronic controlled wind turbines. For frequency response capability, we have derived the impact of DFIG controllers on transient stability and proposed a novel controller to improve contribution to frequency response. For reactive power support, we have derived theoretical limitation of wind turbine generator reactive power capability. Nameplate ratings of the DFIG are limiting factors in the amount of reactive power that can be exchanged with the grid. We find in this project that not all generators are fully utilizing their nameplate capability. Connecting the DFIG rotor terminal to the grid can lead to a shift of frequencies within the machine and can increase the amount of reactive power available for generation. Parameters of the generator impact the preferred connection strategy and we have derived formulas that describe the limits to that end. Frequency response from wind turbines is found to exist with sufficient capability for short-term regulation during generator/load power imbalance. We've shown that controls in popular use today provide degrading impact to frequency response and are not well-suited to fully wind powered systems. We proposed architecture that adds a fast-acting response to complement slower steady-state controls, which improves the existing art of generator control. The added controller is derived from a physics-based model of the DFIG and provides inherent capability of self-stabilizing response. We designed a stability analysis with the combined influence of TQ and FV control, which offers ability to tune the balance of steady-state and transient response. The additional capability brought to wind turbines through this project can improve power system performance. Adopting methods proposed in this project can afford added capability and improve transient response while making more fulfilled use of existing resources.

Future work this project promotes includes a more detailed consideration of generator core design on the impact of a preferred RTC or STC for reactive power capability. The power system planning may be impacted with consideration of primary frequency response guided by improved utility of existing turbines. The ability to specify depth and duration of response using the proposed controller gives flexibility of resources. Resiliency of the power system can be improved with careful consideration and prescription of turbine response. The value of the added capabilities afforded in this project may be identified through consideration of avoided cost of auxiliary compensators and lessened response requirement from other non-wind-powered generators.

References

[1] NERC, "State of reliability," 2017.

[2] "Frequency response standard background document," NERC, 2012.

[3] "Frequency response - issue paper," CAISO, 2015.

[4] "Real Power Balancing Control Performance," NERC Std. BAL-001-2, 2016.

[5] "Frequency Response and Frequency Bias Setting," NERC Std. BAL-003-1.1, 2015.

[6] NERC Resources Subcommittee, "Balancing and frequency control," 2011.

[7] "Generator Frequency and Voltage Protective Relay Settings," NERC Std. PRC-024-2, 2016.

[8] H. J. H. J. Altuve and E. O. S. III, Modern solutions for protection, control, and monitoring of electric power systems, Quality books, Inc., 2010.

[9] "Automatic Underfrequency Load Shedding," NERC Std. PRC-006-2, 2015.

[10] "Undervoltage Load Shedding," NERC Std. PRC-010-2, 2017.

[11] T. M. Haileselassie, R. E. Torres-Olguin, T. K. Vrana, K. Uhlen and T. Undeland, "Main grid frequency support strategy for VSC-HVDC connected wind farms with variable speed wind turbines," in *IEEE Trondheim PowerTech*, 2011.

[12] R. Cardenas, R. Pena, S. Alepuz and G. Asher, "Overview of control systems for the operation of DFIGs in wind energy applications," *IEEE Transactions on Industrial Electronics,* vol. 60, no. 7, pp. 2776-2798, 2013.

[13] N. W. Miller, R. W. Delmerico, K. Kuruvilla and M. Shao, "Frequency responsive controls for wind plants in grids with wind high penetration," in *IEEE Power and Energy Society General Meeting*, 2012.

[14] J. Aho, A. Buckspan, J. Laks, P. Fleming, Y. Jeong, F. Dunne, M. Churchfield, L. Pao and K. Johnson, "A tutorial of wind turbine control for supporting grid frequency through active power control," in *American Control Conference (ACC)*, 2012.

[15] D. Zhi and L. L. Xu, "Direct power control of DFIG with constant switch frequency and improved transient performance," *IEEE Transactions on Energy Conversion*, vol. 22, no. 1, pp. 110-118, 2007.

[16] Y. Liu, L. Jiang, Q. H. Wu and X. Zhou, "Frequency control of DFIG-based wind power penetrated power systems using switching angle controller and AGC," *IEEE Transactions on Power Systems*, vol. 32, no. 2, pp. 1553-1567, 2017.

[17] M. Fazeli and P. P. Holland, "Universal and seamless control of distributed resources-energy storage for all operational scenarios of microgrids," *IEEE Transactions on Energy Conversion,* vol. 32, no. 3, pp. 963-973, 2017.

[18] Y. Tan, L. Meegahapola and K. M. Muttaqi, "A suboptimal power-point-tracking-based primary frequency response strategy for DFIGs in hybrid remote area power supply systems," *IEEE Transactions on Energy Conversion,* vol. 31, no. 1, pp. 93-105, 2016.

[19] Y. Li, Z. Xu, J. Ostergaard and D. J. D. J. Hill, "Coordinated control strategies for offshore wind farm integration via VSC-HVDC for system frequency support," *IEEE Transactions on Energy Conversion,* vol. 32, no. 3, pp. 843-856, 2017.

[20] I. Erlich, A. Korai, T. Neumann, M. K. Zadeh, S. Vogt, C. Buchhagen, C. Rauscher, A. Menze and J. Jung, "New control of wind turbines ensuring stable and secure operation following islanding of wind farms," *IEEE Transactions on Energy Conversion*, vol. 32, no. 3, pp. 1263-1271, 2017.

[21] S. Sharma, B. Singh, A. Chandra and K. Al-Haddad, "Control of doubly fed induction generator in standalone wind energy conversion system," in *IEEE Industry Applications Society Annual Meeting*, 2015.

[22] T. Ahmad, T. Littler and W. Naeem, "An active PID-based inertial control of a doubly-fed induction generator," in *27th Irish Signals and Systems Conference (ISSC)*, 2016.

[23] M. N. a. S. Farhangi, "Voltage and frequency stability for control of stand-alone DFIG-based wind turbine using direct voltage control method," in *14th International Conference on Environment and Electrical Engineering*, 2014.

[24] M. H. Variani and K. Tomsovic, "Two-level control of doubly fed induction generator using flatness-based approach," *IEEE Transactions on Power Systems*, vol. 31, no. 1, pp. 518-525, 2016.

[25] P. Cheng, H. Nian, C. Wu and Z. Q. Zhu, "Direct stator current vector control strategy of DFIG without phase-locked loop during network unbalance," *IEEE Transactions on Power Electronics*, vol. 32, no. 1, pp. 284-297, 2017.

[26] G. Lalor, J. Ritchie, S. Rourke, D. Flynn and M. J. O'Malley, "Dynamic frequency control with increasing wind generation," in *IEEE Power Engineering Society General Meeting*, 2004.

[27] North American Electric Reliability Corporation, "Essential reliability services," Dec 2015. [Online]. Available: http://www.nerc.com/pa/RAPA/ra/Reliability\%20Assessments%20DL/ERS%20Abstract%20Report%20Final.pdf.

[28] S. A. Newell, R. Carroll, P. Ruiz and W. Gorman, "Cost-benefit analysis of ERCOT's future ancillary services proposal," ERCOT, 2015.

[29] L. Yang, Z. Xu, J. Ostergaard, Z. Y. Dong and K. P. Wong, "Advanced control strategy of DFIG wind turbines for power system fault ride through," *IEEE Transactions on Power Systems*, vol. 27, no. 2, pp. 713-722, 2012.

[30] VEM Motors GmbH, "Overview wind power generators, synchronous and asynchronous generator, yaw drives," [Online]. Available: http://www.vem.fi/userData/vem/downloads/vem-motors-gmbh/tuoteluettelot/Product-overview-VEM-Windpower.pdf. [Accessed 2 May 2018].

[31] RTE-France, "A study of theoretical reactive power capacity of a wind turbine based on an asynchronous double-fed machine,," 2014.

[32] P. C. Krause, O. Wasynczuk and S. D. Sudhoff, Analysis of Electric Machinery, IEEE Press, 1995.

[33] N. David and D. Aliprantis, "Improved efficiency of DFIG wind energy conversion systems by operating in the rotor-tied configuration," *Electrical Machines (ICEM), 2014 International Conference on*, pp. 189-195, 2014.

[34] H. Vickers, The induction motor; the theory, design, and application of alternating-current machines including fractional H.P. motors., 2nd ed., London: Pitman, 1953.

[35] Y.-M. You, T. A. Lipo and B. I. Kwon, "Design and analysis of a novel grid-connected to rotor type doubly fed induction machine," *IEEE Transactions on Magnetics,* vol. 48, no. 2, pp. 919-922, 2012.

[36] N. David and D. Aliprantis, "DFIG with grid-connected rotor for wind energy conversion system," in *Electric Machines Drives Conference (IEMDC), 2013 International*, 2013.

[37] "8231-00 three-phase wound-rotor induction machine," a product datasheet prepared by Festo Didactic, 2017.

[38] S. Seman, J. Niiranen, S. Kanerva, A. Arkkio and J. Saitz, "Performance study of a doubly fed wind-power induction generator under network disturbances," *IEEE Trans. Energy Conversion,* vol. 21, no. 4, pp. 883-890, 2006.

[39] M. Singh and S. Santoso, "Dynamic models for wind turbines and wind power plants," NREL, 2011.

[40] M. Bongiorno and T. Thiringer, "A generic DFIG model for voltage dip ride-through analysis," *IEEE Trans. Energy Conversion,* vol. 28, no. 1, pp. 76-85, 2013.

[41] Vestas Wind Systems A/S, "2 MW V90-1.8/2.0 MW," a product brochure, 2012.

[42] O. Anaya-Lara, N. Jenkins, J. Ekanayaka, P. Cartwright and M. Hughes, Wind energy generation modeling and control, John Wiley & Sons, Ltd, 2009.

[43] B. Wu, Y. Lang, N. Zargari and S. Kouro, Power conversion and control of wind energy systems, John Wiley & Sons, Ltd, 2011.

[44] N. David, The doubly-fed induction generator in the rotor-tied configuration, Master's thesis, Iowa State University, 2014.

[45] E. Loukarakis, I. Margaris and P. Moutis, "Frequency control support and participation methods provided by wind generation," in *Electrical Power Energy Conference (EPEC)*, 2009.

[46] L. Shang, J. Hu, X. Yuan and Y. Chi, "Understanding inertial response of variable-speed wind turbines by defined internal potential vector," *Energies,* vol. 10, no. 22, pp. 1-17, 2016.

[47] J. Liu, Y. Y. Miura and T. T. Ise, "Comparison of dynamic characteristics between virtual synchronous generator and droop control in inverter-based distributed generators," *IEEE Transactions on Power Electronics,* vol. 31, no. 5, pp. 3600-3611, 2016.

[48] M. Guan, W. Pan, J. Zhang, Q. Hao, J. Cheng and X. Zheng, "Synchronous generator emulation control strategy for voltage source converter (VSC) stations," *IEEE Transactions on Power Systems*, vol. 30, no. 6, pp. 3093-3101, 2015.

[49] N. K. S. Naidu and S. B., "Experimental implementation of doubly fed induction generator-based standalone wind energy conversion system," *IEEE Transactions on Industry Applications,*, vol. 52, no. 4, pp. 3332-3339, 2016.